

Discovery of Tetrahydroquinoxalines as Bromodomain and Extra-Terminal Domain (BET) Inhibitors with Selectivity for the Second Bromodomain

Robert P. Law, Stephen J. Atkinson, Paul Bamborough, Chun-wa Chung, Emmanuel H Demont, Laurie J. Gordon, Matthew Lindon, Rab K. Prinjha, Allan J. B. Watson, and David Jonathan Hirst

J. Med. Chem., **Just Accepted Manuscript** • DOI: 10.1021/acs.jmedchem.7b01666 • Publication Date (Web): 15 Apr 2018

Downloaded from <http://pubs.acs.org> on April 15, 2018

Just Accepted

"Just Accepted" manuscripts have been peer-reviewed and accepted for publication. They are posted online prior to technical editing, formatting for publication and author proofing. The American Chemical Society provides "Just Accepted" as a service to the research community to expedite the dissemination of scientific material as soon as possible after acceptance. "Just Accepted" manuscripts appear in full in PDF format accompanied by an HTML abstract. "Just Accepted" manuscripts have been fully peer reviewed, but should not be considered the official version of record. They are citable by the Digital Object Identifier (DOI®). "Just Accepted" is an optional service offered to authors. Therefore, the "Just Accepted" Web site may not include all articles that will be published in the journal. After a manuscript is technically edited and formatted, it will be removed from the "Just Accepted" Web site and published as an ASAP article. Note that technical editing may introduce minor changes to the manuscript text and/or graphics which could affect content, and all legal disclaimers and ethical guidelines that apply to the journal pertain. ACS cannot be held responsible for errors or consequences arising from the use of information contained in these "Just Accepted" manuscripts.



Discovery of Tetrahydroquinoxalines as Bromodomain and Extra-Terminal Domain (BET) Inhibitors with Selectivity for the Second Bromodomain

*Robert P. Law^{†**}, Stephen J. Atkinson[†], Paul Bamborough[§], Chun-wa Chung[§], Emmanuel H. Demont[†], Laurie J. Gordon[§], Matthew Lindon[†], Rab K. Prinjha,[†] Allan J.B. Watson[‡], David J. Hirst[†].*

[†]Epigenetics Discovery Performance Unit, [§]Platform Technology and Science,
GlaxoSmithKline, Medicines Research Centre, Stevenage, Hertfordshire, SG1 2NY, U.K.

[‡]WestCHEM, Department of Pure and Applied Chemistry, University of Strathclyde, Thomas
Graham Building, 295 Cathedral Street, Glasgow, G1 1XL, U.K.

ABSTRACT

The bromodomain and extra-terminal domain (BET) family of proteins bind acetylated lysine residues on histone proteins. The four BET bromodomains, BRD2, BRD3, BRD4 and BRDT, each contain two bromodomain modules. BET bromodomain inhibition is a potential therapy for various cancers and immunoinflammatory diseases, but few reported inhibitors show selectivity within the BET family. Inhibitors with selectivity for the first or second bromodomain are desired to aid investigation of the biological function of these domains. Focused library screening identified a series of tetrahydroquinoxalines with selectivity for the second bromodomains of the BET family (BD2). Structure-guided optimization of the template improved potency, selectivity and physicochemical properties, culminating in potent BET inhibitors with BD2 selectivity.

INTRODUCTION

Bromodomain containing proteins (BRDs) are epigenetic ‘reader’ proteins, an important class of translation mediators which bind to acetylated lysine (KAc) residues on the N-terminal tails of histones and recruit transcriptional regulator complexes to chromatin.¹⁻⁴ To date, 46 human proteins have been found to contain one or more bromodomain motifs, with 61 distinct bromodomains identified.⁵ The bromodomain and extra-terminal (BET) family of proteins consists of BRD2, BRD3, BRD4, and BRDT, each of which contain two bromodomains (BD1 and BD2). The four BD1 domains show a high degree of structural homology, as do the four BD2 domains.²

BRD2, 3, and 4 are ubiquitously expressed, whereas BRDT is confined to the testes and ovaries and is crucial for spermatogenesis.⁶⁻⁸ BET BRDs recruit RNA polymerase II to chromatin and polymerase-associated factor complex (PAFc) complexes,⁹⁻¹⁰ thus initiating

transcription. BRD4 also binds positive transcription elongation factor (PTEF-b) through its C-terminal domain, causing transcriptional elongation.¹¹

Dysregulation of BET family members has been linked to diverse disease phenotypes.^{1-2, 5}

BET proteins facilitate the transcription of tumor growth-promoting and anti-apoptotic genes,¹² including c-Myc,¹³ which is activated by super-enhancer regions that recruit BRD4 at higher than normal levels.¹⁴ The squamous cell epithelial cancer nuclear protein *in testis* (NUT) midline carcinoma (NMC) is driven by the formation of a BRD4-NUT fusion oncogene;¹⁵ small-molecule BRD4 inhibition caused growth arrest and apoptosis in NMC cells.¹⁶ Small-molecule BET inhibitors have shown efficacy against a range of cancers,¹⁷⁻²⁰ and several inhibitors have entered clinical trials in oncology.²¹

BET inhibition has been shown to potently modulate inflammatory autoimmune gene expression.²²⁻²³ BET bromodomains control the differentiation of CD4+ T cells to inflammatory Th17 cells through genomic localization and their effects on cytokine regulation.²⁴ Treatment of naïve CD4+ cells with BET bromodomain inhibitors suppressed expression of proinflammatory cytokines whilst also upregulating anti-inflammatory gene products, mimicking cMyc inhibition.²⁵ In human monocytes, BET inhibition suppressed the transcriptional response of the Janus kinase/signal transducers and activators of transcription (JAK-STAT) pathway to cytokine stimulation,²⁶ downregulated pro-inflammatory cytokine production in dendritic cells,²⁷ macrophages,²⁸ and rheumatoid arthritis synovial fibroblasts.²⁹ *In vivo*, BET inhibitors have shown therapeutic anti-inflammatory effects in rodent models of acute sepsis,³⁰ periodontitis,³¹ psoriasis,³² arthritis³³ and pathologic bone loss.³⁴ Furthermore, BET inhibitors have been shown to reactivate human immunodeficiency virus (HIV) from latency,^{11, 35-37} and are in clinical investigation for the treatment of atherosclerosis.³⁸⁻³⁹

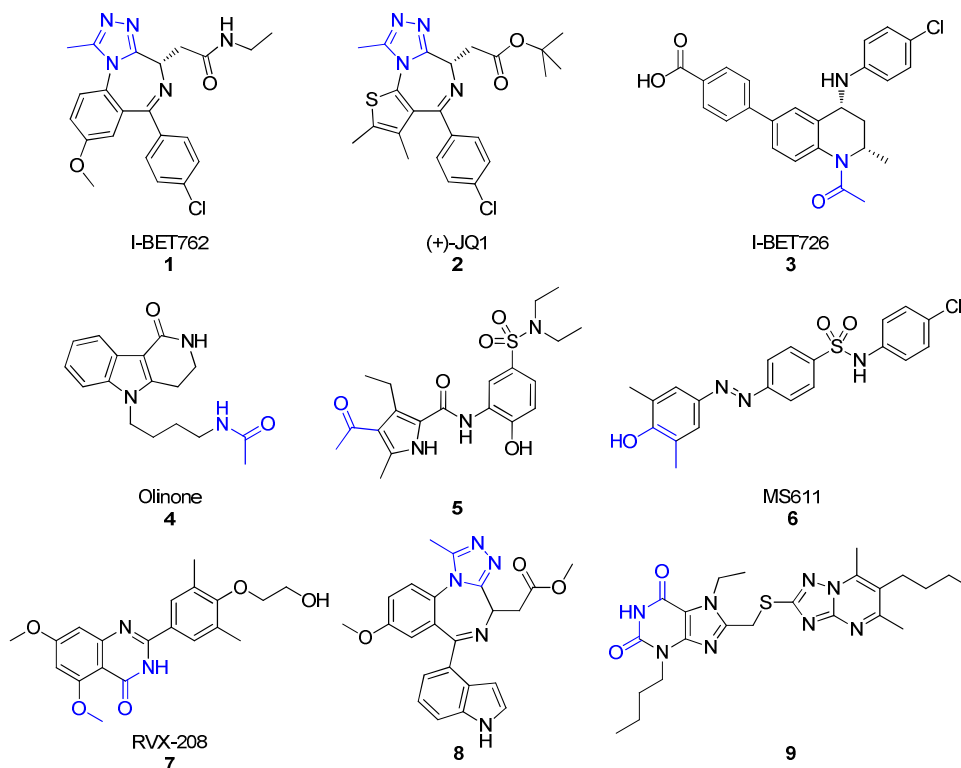


Figure 1. Selected BET inhibitors. Acetylated lysine mimetics are highlighted.

Diverse BET inhibitor scaffolds have been reported to interact with the KAc binding site (Figure 1).^{5, 21, 40-42} All feature a KAc mimic which binds to a conserved Asn residue in a similar manner to the native N-acetyl peptide. Among BET inhibitors, the triazolodiazepine chemotype has been extensively explored, as exemplified by the clinical compound I-BET762 (**1**)^{30, 43-44} and widely-used probe JQ1 (**2**).¹⁶ Additionally, the tetrahydroquinoline I-BET726 (**3**)⁴⁵ was discovered through phenotypic screening of Apolipoprotein A1 (ApoA1) upregulators, and subsequently shown to function as a BET bromodomain inhibitor. **1-3** are pan-BET inhibitors which exhibit little or no selectivity between the 8 bromodomains of the BET family. Whilst more selective inhibitors are less well explored, there has been recent progress in this field (*vide infra*).

While the sequence homology of the four dual-BRD BET bromodomains is high, differences exist between the BD1 and BD2 domains which allow selectivity to be achieved (Figure 2). For BRD4, the ‘gatekeeper’⁴⁶ residue, which restricts access to the Trp-Pro-Phe -bordered region termed the WPF shelf, switches between I146 in BD1 and V439 in BD2, with a Q85/K378 switch at the base of the ZA channel. The greatest differences lie in the BC loop, with D144 in BD1 exchanged for H437 in BD2 and an aspartic to glutamic acid switch of the adjacent residue. Similar differences exist between BD1 and BD2 amongst BRD2/3/T, as shown in the sequence alignment in Figure 2.

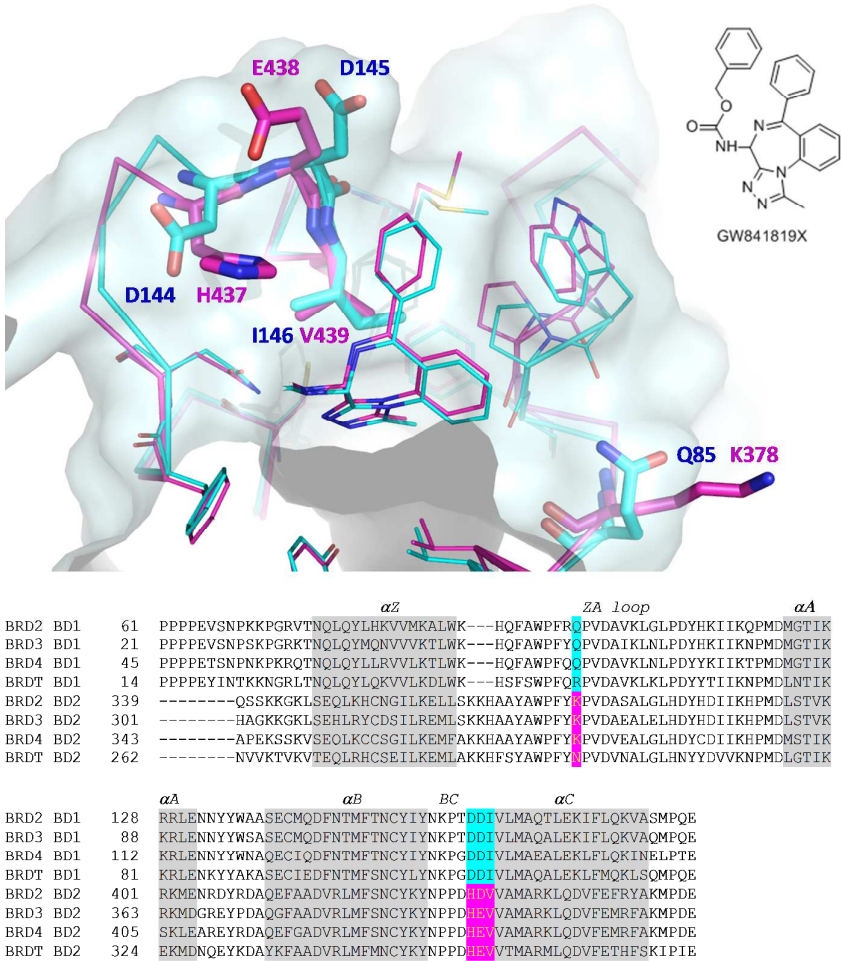


Figure 2. Top: Comparison of BRD4 BD1 (2YEL, cyan) and BD2 (2YEM, magenta) with triazolodiazepane GW841819X bound.⁴⁷ Surface over the BD1 protein (pale cyan) has been

shown to highlight key residue differences in the BC loop (D144/H437; D145/E438), ZA channel (Q85/K378) and the gatekeeper residues (I146/V439) between BRD4 BD1 (blue residue labels) and BD2 (magenta residue labels). Bottom: Sequence alignment of BET bromodomains with the residues highlighted.

Olinone (**4**) utilizes a clash with the BD2-specific H437 to obtain 3.4 μM affinity for BRD4 BD1 with no BRD4 BD2 activity detected,⁴⁸ while the acylpyrrole **5** showed 0.24 μM affinity for BRD4 BD1 with 10-fold selectivity over other members of the BET family.⁴⁹ The diazobenzene MS611 (**6**), in which the phenol forms the KAc mimetic, also showed BRD4 BD1 $K_D = 0.41 \mu\text{M}$ and 100-fold selectivity over BRD4 BD2.^{46, 48} RVX-208 (**7**), currently in Phase III clinical trials for cardiovascular diseases,³⁹ was elucidated to be a BET inhibitor with $K_D = 4 \mu\text{M}$ and ~ 20 -fold selectivity for BRD3 BD2 over BRD3 BD1,^{38, 50} additional analogues of this series have also shown BD2-selectivity and therapeutic effects *in vivo*.⁵¹⁻⁵² The selectivity is postulated to be due to differences in the structural dynamics of the BD1/BD2 ZA loop regions, with **7** increasing contact between the ZA and BC loops in BD2, and interaction of **7** with the BD2-specific His.⁵³⁻⁵⁴ Using a ‘bump-and-hole’ chemical biology strategy with mutant bromodomain modules and suitably modified inhibitors, Ciulli *et al.* engineered domain selective inhibition.⁵⁵⁻⁵⁶ During this work, it was observed that the indole **8** displayed 20-fold selectivity for wild-type BRD2 BD2 over BRD2 BD1, though this was reduced to ~ 10 -fold at BRD4. The domain selectivity was attributed to improved edge-to-face interactions of the indole ring with the BD2-specific His, compared to the chlorophenyl of **1**.⁵⁶ Weak (~ 6 -fold) BRD4 BD2 bias was also observed for the benzoisoxazoloazepine inhibitor CPI-0610, currently in Phase I clinical trials.⁵⁷ In the patent literature, Abbvie have disclosed compounds with selectivity for both BRD4 BD1 and BD2,⁵⁸ with structures related to the pyrrolopyridone ABBV-075/mivebresib.⁵⁹

In an intriguing example of single BET bromodomain specificity, the xanthine derivative **9** exhibited 5 μ M affinity for BRD4 BD1 with 10-fold bias over other BD1 domains and no detectable BD2 binding. Differences in the dynamic movement of the ZA loop were hypothesized as the cause of selectivity.⁶⁰

These chemical tools have begun to provide insight into the roles of individual domains. Using a mutated BRD4 bromodomain, the bump-and-hole strategy demonstrated that inhibition of BD1 alone was able to prevent chromatin binding to BRD4.⁵⁶ Selective BD1 inhibition with **4** promoted oligodendrocyte progenitor differentiation; whilst in contrast, pan-BET inhibition hindered it.⁴⁸ In a HepG2 cell line **7** weakly displaced BRD3 from chromatin, and affected only a small subset of genes compared to JQ1 (**2**). Furthermore, **7** was unable to produce a strong transcriptional response in a subset of these genes,³⁸ and had no effect on oligodendrocyte progenitor differentiation.⁴⁸

These initial studies indicate that domain selective inhibition may exhibit differentiated pharmacology compared to pan-BET inhibition, yet BD2 selective inhibitors are poorly explored. In addition, the phenotypic effect of a small molecule target should ideally be confirmed with multiple chemically distinct series,⁶¹ but the potency and selectivity of **7-8** are limited. To corroborate these emerging results and further investigate the biological role of BD2, additional BD2-selective BET inhibitors are desired from alternative chemotypes with improved potency and selectivity.

RESULTS AND DISCUSSION

Discovery of the Tetrahydroquinoxaline Scaffold.

A previous fragment-based screen carried out in our laboratories identified tetrahydroquinoline **10** (Figure 3) which bound weakly but with high ligand efficiency (LE) to BRD2-4.⁶² Separately, optimization of the tetrahydroquinoline scaffold *via* phenotypic

assays identified appropriate vectors for potency, culminating with **3**, which was subsequently identified as a pan-BET inhibitor (pIC_{50} BRD4 BD1 = 7.8 and BD2 = 8.2).⁴⁵ This work led to the investigation of similar chemotypes for BET bromodomain binding.

Tetrahydroquinoxalines **11-13**, also upregulators of ApoA-1, were screened against both bromodomains of BRD4 in fluorescence resonance energy transfer (FRET) assays, and showed encouraging potency, LE and BD2 selectivity. At the outset of this work, these represented novel BET inhibitor chemotypes; the acyltetrahydroquinoxaline template including **12** was also independently optimized by Forma Therapeutics,⁶³ culminating in a series of 1,4-diacyl tetrahydroquinoxaline pan-BET inhibitors.⁶⁴ In addition, the structurally distinct tetrahydroquinoline scaffold of **10** has been investigated by both ourselves and others to afford BET inhibitors with variable selectivity towards the BD2 domains.^{21, 65-66}

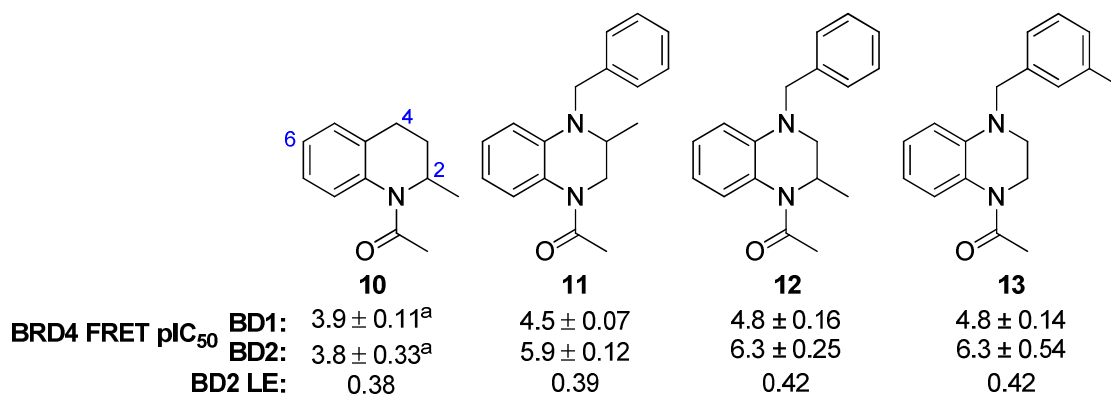


Figure 3. Structures and potencies of initial hit compounds. pIC_{50} data is $n=4$ or greater

unless stated. Ranges shown are standard deviations. a) $n=2$.

We obtained an X-ray structure of **13** bound to BRD4 BD2 (Figure 4), which showed the acetyl group of **13** behaving as the KAc mimetic, as seen for **3**. The amide carbonyl formed hydrogen bonds to N433 and a through-water interaction to Y390. The tolyl group is placed between the WPF stack (W374, P375 and F375) and the BD2-specific H437 mimetic in a similar manner to **3**. Given that **3** occupies the WPF shelf yet is a pan-BET inhibitor, the

differing angle of the ring in **13** may be crucial for BD2 selectivity. The unsubstituted tetrahydroquinoxaline ring of **13** can be seen to pucker towards a small lipophilic pocket, as occupied by the methyl group of **3**. Finally, THQ **3** derives additional potency by deploying a 6-aryl group into the ZA channel. This is almost identical in BD1 and BD2 and additional lipophilic binding and π -interactions with the WPF tryptophan led to a similar increase in potency at both domains.

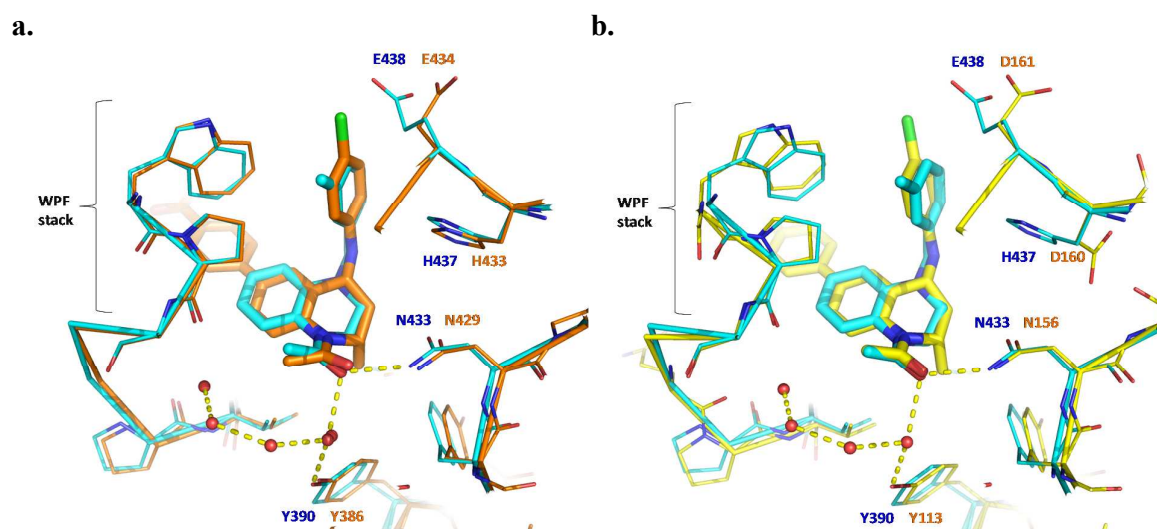


Figure 4. a) X-ray crystal structures of **13** bound to BRD4 BD2 (cyan, PDB code:6FFD, 1.83 Å, blue residue labels), overlaid with I-BET726 (**3**) bound to BRD2 BD2 (orange, PDB code: 4UYG, 2.5 Å, orange residue labels). **b)** **13** bound to BRD4 BD2 (cyan, 1.83 Å, blue residue labels), overlaid with I-BET726 (**3**) bound to BRD2 BD1 (yellow, PDB code: 4UYF, 1.6Å, orange residue labels).

As such, there appeared three main vectors for optimization of **11-13** into a BD2 selective tool. Firstly, the small lipophilic pocket would be explored with a screen of small alkyl groups at the 2-position of the tetrahydroquinoxaline ring. Alternative substitution patterns of the phenyl ring interacting with the WPF shelf would be screened, to probe their influence on

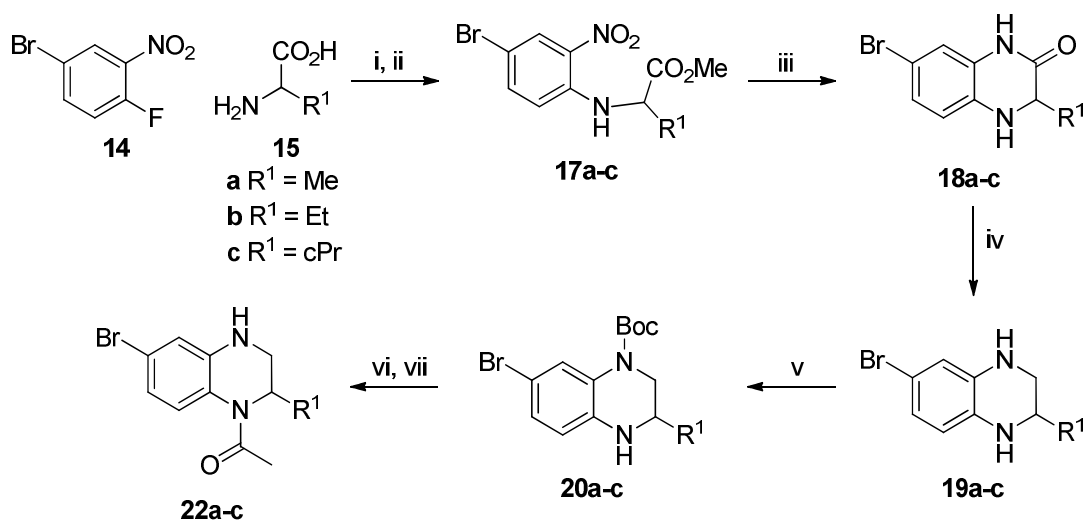
selectivity. Lastly, the ZA channel would be explored. It was expected that targeting this site would not increase selectivity, but could enhance potency, as seen for **3**.⁴⁵

We set out to investigate these vectors individually, before combining the optimal substituents to give final compounds. Optimization was initially carried out on racemic compounds, with the role of individual enantiomers investigated once potent and selective compounds were obtained (*vide infra*).

Synthetic Chemistry

A strategy of late-stage diversification was chosen to enable rapid library synthesis (Scheme 1). To access the tetrahydroquinoxaline core where R¹ = Me, Et or cPr, a S_NAr reaction between fluorobenzene **14** and amino acids **15** gave the amino esters **17** after esterification. Reduction of the nitro group and cyclisation with SnCl₂ gave quinoxalinones **18**, which could be reduced to tetrahydroquinoxalines **19** with borane. The steric bulk of the 2-substituent and electron-withdrawing nature of the bromide allowed differentiation between the two amines, with Boc-protection affording **20** as the major product. Acetylation followed by Boc deprotection gave **22**, with synthetic handles at the 4- and 6-positions.

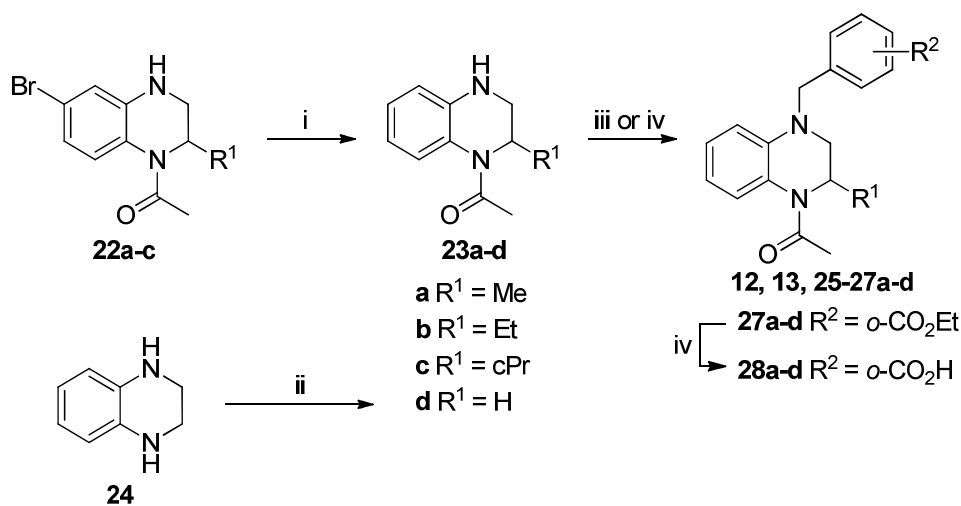
Scheme 1. Representative synthesis of building blocks **22a-c**.^a



^aReagents and conditions: (i) K₂CO₃, DMF, 80 °C; (ii) SOCl₂, MeOH, reflux, 70-82% over two steps; (iii) SnCl₂, EtOH, reflux, 90-97%; (iv) BH₃•THF, THF, 60 °C, 90-95%; (v) Boc₂O, DMAP, Et₃N, DCM, rt, 53-69%; (vi) Ac₂O, Et₃N, DCM, reflux, 51-89%; (vii) HCl, DCM, -20 °C, 62-90%.

To access compounds lacking a 6-substituent with a variety of alkyl groups at the 2-position, the 6-Br moiety was removed by hydrogenation to give **23a-c** (Scheme 2). The 2-H analogue **23d** was synthesized by acetylation of tetrahydroquinoxaline **24**. Reductive amination or S_N2 displacement of a benzylic bromide gave the target compounds. For examples bearing a benzoic acid, the coupling reaction was undertaken using the corresponding ethyl esters and the product hydrolyzed to afford the final compounds **28a-d**.

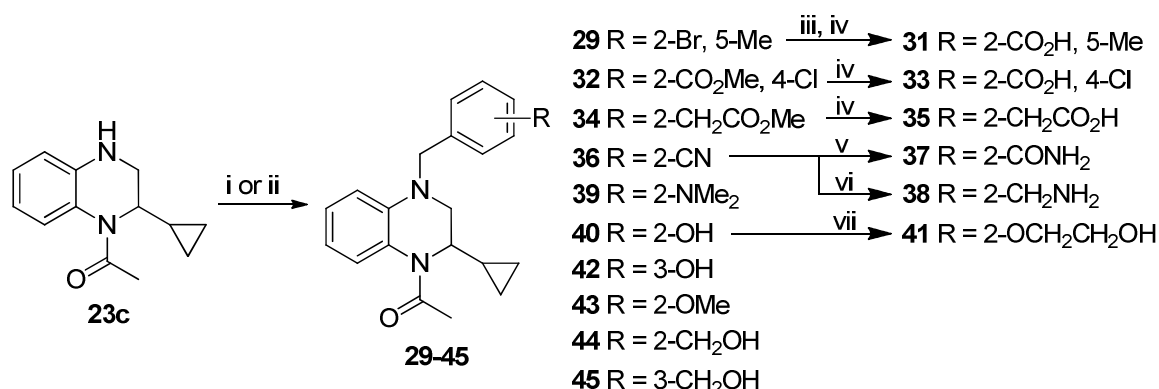
Scheme 2. Representative synthesis of 6-H compounds.^a



^aReagents and conditions: (i) Flow hydrogenation, 10% Pd/C, H₂, MeOH, rt, 93-97%; (ii) Ac₂O, EtOH, 0 °C – rt, 95%; (iii) Benzylic bromide, K₂CO₃, DMF, 90 - 110 °C, 17-79%; (iv) Aryl aldehyde, NaBH(OAc)₃, DCM, rt, 43%; (iv) LiOH, H₂O, MeOH, THF, rt, 40-73%.

To explore the WPF shelf, a set of analogues bearing a 2-cPr substitution were designed. These could be accessed from **23c** in a similar manner (Scheme 3). The trisubstituted benzoic acid **31** was synthesized by Pd-catalyzed carbonylation-esterification of the corresponding bromide **29** with Mo(CO)₆, followed by saponification of the resulting ester to give **31**. The nitrile **36** was converted to the primary amide **37** using H₂O₂ and K₂CO₃ and to the benzylamine **38** by hydrogenation over Raney Ni. Phenol **40** was alkylated with 2-bromoethanol to afford the hydroxyethanol analogue **41**.

Scheme 3. Synthesis of WPF shelf array.^a

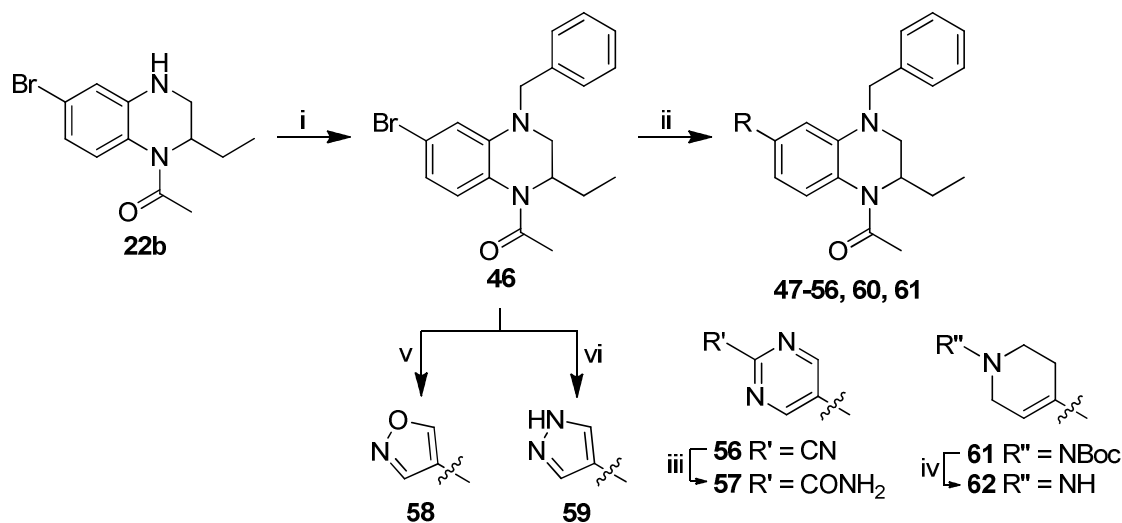


^aReagents and conditions: (i) Benzylic bromide, K₂CO₃, DMF, 90-110 °C, 42-85%; (ii) Benzylic aldehyde, NaBH(OAc)₃, DCM, rt, 21-85%; (iii) Mo(CO)₆, Herrmann's catalyst, DIPEA, 1-butanol, 1,4-dioxane, μ W, 150 °C, 26%; (iv) LiOH, H₂O, MeOH, THF, rt, 58-83%; (v) H₂O₂, K₂CO₃, DMSO, rt, 77%; (vi) Flow hydrogenation, Raney Ni, 50 bar H₂, EtOH, 50 °C, 32%; (vii) 2-Bromoethanol, K₂CO₃, DMF, 110 °C, 50%.

6-Aryl compounds were synthesized *via* benzylation of 2-Et,6-Br tetrahydroquinoxaline **22b** to give **46**, followed by Suzuki-Miyaura coupling (Scheme 4). Amidopyrimidine **57** was synthesized by H₂O₂/K₂CO₃ oxidation of nitrile **56**. For 5-membered heterocycles yields with

Pd(dppf)Cl₂/Cs₂CO₃ were low, and modified conditions were used for isoxazole **58** and pyrazole **59**. The use of the Boc-protected pyrazole improved the stability of the boronic ester, with the Boc-group being removed from the product under the reaction conditions. The *N*-Boc tetrahydropyridine **61** was deprotected with TFA to give **62**.

Scheme 4. Synthesis of 6-aryl compounds.^a

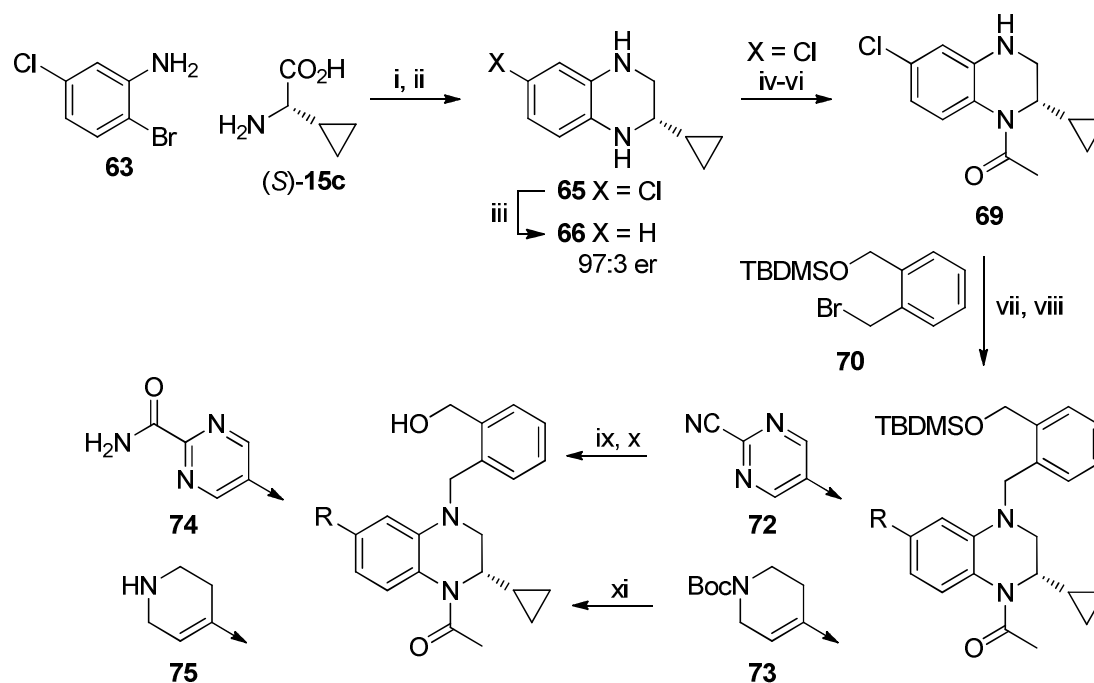


^aReagents and conditions: (i) BnBr, K₂CO₃, DMF, 90 °C, 56%; (ii) ArB(OH)₂ or ArBPin, Pd(dppf)Cl₂, Cs₂CO₃, 1,4-dioxane, H₂O, μW, 110 °C, 7-96%; (iii) H₂O₂, K₂CO₃, DMSO, rt, 70%; (iv) TFA, DCM, rt, 96%; (v) Isoxazole-4-boronic acid pinacol ester, Pd(dppf)Cl₂, DIPEA, 1,4-dioxane, H₂O, μW, 110 °C, 43%; (vi) (1-(Boc)-1H-pyrazol-4-yl)boronic acid pinacol ester, Pd₂(dba)₃, XPhos, K₃PO₄, 1-butanol, μW, 115 °C, 38%.

Only one enantiomer of fragment hit **10** was seen to crystallize in BRD4 BD1,⁶² and separation of the two enantiomers of **44** by preparative chiral high performance liquid chromatography (HPLC) showed only one enantiomer had significant activity (Table 2). This was assumed to be the (*S*)-enantiomer based on the structure of **3** and crystallography of **10** (Figure 4), as such single enantiomer quinoxalinones were synthesized (Scheme 5). Cu-catalyzed Ullman coupling-cyclisation of bromoaniline **63** and (*S*)-cyclopropylglycine (*S*)-

15c⁶⁷ gave the quinoxalinone core (**64**),⁶⁸ which was reduced to **65**. To confirm enantiopurity at this stage, **65** was hydrogenated to **66** for comparison with racemic material, and exhibited 97:3 *er* by chiral HPLC. Protection followed by acetylation and deprotection gave **69**, followed by alkylation with benzylic bromide **70**. This route necessitated the use of a 6-Cl substituent to avoid regiochemical issues during the Ullmann coupling, consequently a reassessment of the Suzuki-Miyaura coupling conditions was required. BrettPhos G3 palladacycle produced efficient coupling to afford pyrimidine **72** and tetrahydropyridine **73**. Removal of the TBDMS protecting group from **72** with TBAF, followed by nitrile oxidation gave the pyrimidine amide **74**, while global deprotection of **73** with HCl afforded the tetrahydropyridine **75**. Chiral HPLC of **75** (see Supporting Information) showed no racemization had occurred during the synthesis.

Scheme 5. Synthesis of single enantiomer products.^a



^aReagents and conditions: (i) CuCl, DMEDA, DBU, DMSO, 110 °C, 73%; (ii) BH₃•THF, THF, 60 °C, 79%; (iii) 10% Pd/C, H₂, EtOH, rt, 100%; (iv) Boc₂O, DMAP, Et₃N, DCM, rt, 85%; (v) Ac₂O, Et₃N, 2-MeTHF, reflux; (vi) TFA, DCM, rt, 82% over two steps; (vii) **70**, NaH, DMF, 0 °C – rt, 80%; (viii) R-BPin, BrettPhos Pd G3, Cs₂CO₃, DME, 110 °C, μ W, 2 h, 43-69%; (ix) TBAF, THF, rt, 88%; (x) H₂O₂, K₂CO₃, DMSO, rt, 46%; (xi) HCl, MeOH, rt, 47%.

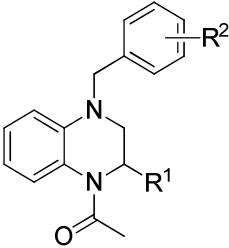
Medicinal Chemistry

We began our optimization campaign by altering the 2-substituent and WPF-shelf binding motif. We postulated that a small alkyl substituent at the 2-position of the core could improve potency due to the proximity of the WPF shelf-occupying aryl ring to the basic histidine (Figure 4), and an acidic group could boost selectivity through an ionic interaction. To test these hypotheses, 2-substituents were screened, each with a phenyl, *m*-tolyl or *o*-benzoic acid WPF shelf group (Table 1).

In our hands, RVX-208 (**7**) exhibited ~4-fold selectivity for BRD4 BD1 over BRD4 BD2 (Table 1 and Table S1), consistent with previous reports,³⁸ while the tetrahydroquinoxaline examples showed good potency and higher selectivity at BRD4 BD2. Initially, it was pleasing to observe a 0.5 log increase in BD2 potency with the addition of a *m*-methyl group to the shelf aryl group (**13** vs **25d**) in the absence of an R¹ substituent. Furthermore, the addition of an R¹ = Me vs H, substituent also led to a similar increase in potency when the shelf group was phenyl (**12** vs **25d**). Disappointingly, combining the methyl groups of **12** and **13** to give **26a** did not improve potency, suggesting these two positions could not always be optimized independently. The benzoic acid moiety (**28a-d**) generally did not produce a significant increase in BD2 potency but did decrease BD1 potency. Furthermore, increasing the size of the R¹ substituent proved beneficial - methyl (**a**) and ethyl (**b**) groups were broadly

similar, with ethyl examples showing marginally higher potency but lower selectivity. However, a cyclopropyl group (**c**) conferred good selectivity across all three substituents; the 2-cyclopropyl acid **28c** had BD1 potency below the detectable limit of the FRET assay (50 μ M), giving a BD2 selectivity of >63-fold. Despite the unusually high potency and selectivity of **13** amongst the 2-H examples, in general substitution at the 2-position was required for acceptable potency. Apart from benzoic acids **28a-d**, all compounds were highly lipophilic at pH 7.4 as measured by chromatographic LogD (ChromLogD_{7.4}),⁶⁹ and we set reduction of lipophilicity as an additional optimization goal in order to improve developability parameters.⁷⁰

Table 1. Biochemical potency and lipophilicity of initial screen of 2-substituents and WPF shelf binding groups.

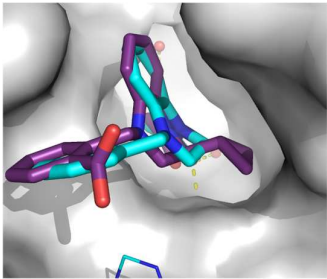
						
Cmpd	R ¹	R ²	BRD4 FRET pIC ₅₀ ^a		BD2	
			BD1	BD2	Selectivity (fold)	ChromLogD _{7.4}
(+JQ1 (2))	-	-	7.4 ± 0.23	7.3 ± 0.19	-	7.3
I-BET726 (3)	-	-	7.8 ± 0.10	8.2 ± 0.13	3	3.9
RVX-208 (7)	-	-	5.2 ± 0.01	5.8 ± 0.06	4	2.9

25d		H	5.0 ± 0.07	5.6 ± 0.04	4	5.6
13	H	<i>m</i> -Me	4.8 ± 0.14	6.3 ± 0.54	32	5.9
28d		<i>o</i> -CO ₂ H	$<4.3^b$	5.3 ± 0.07	>10	1.2
12		H	4.8 ± 0.16	6.3 ± 0.25	32	5.9
26a	Me	<i>m</i> -Me	4.7 ± 0.05	6.0 ± 0.08	20	6.5
28a		<i>o</i> -CO ₂ H	4.4^b	5.8 ± 0.05	25	1.5
25b		H	5.0 ± 0.15	6.2 ± 0.03	16	6.5
26b	Et	<i>m</i> -Me	4.9 ± 0.06	6.1 ± 0.03	16	7.1
28b		<i>o</i> -CO ₂ H	4.5 ± 0.17	6.1 ± 0.07	40	1.9
25c		H	4.7 ± 0.07	6.2 ± 0.05	32	6.7
26c	cPr	<i>m</i> -Me	4.6 ± 0.03	6.1 ± 0.08	32	7.2
28c		<i>o</i> -CO ₂ H	$<4.3^c$	6.1 ± 0.04	>63	2.2

Ranges shown are standard deviations. *a*) All compounds are n = 3 or greater. *b*) Below assay detection limit (50 μ M). *c*) <4.3 on two additional test occasions.

a)

b)



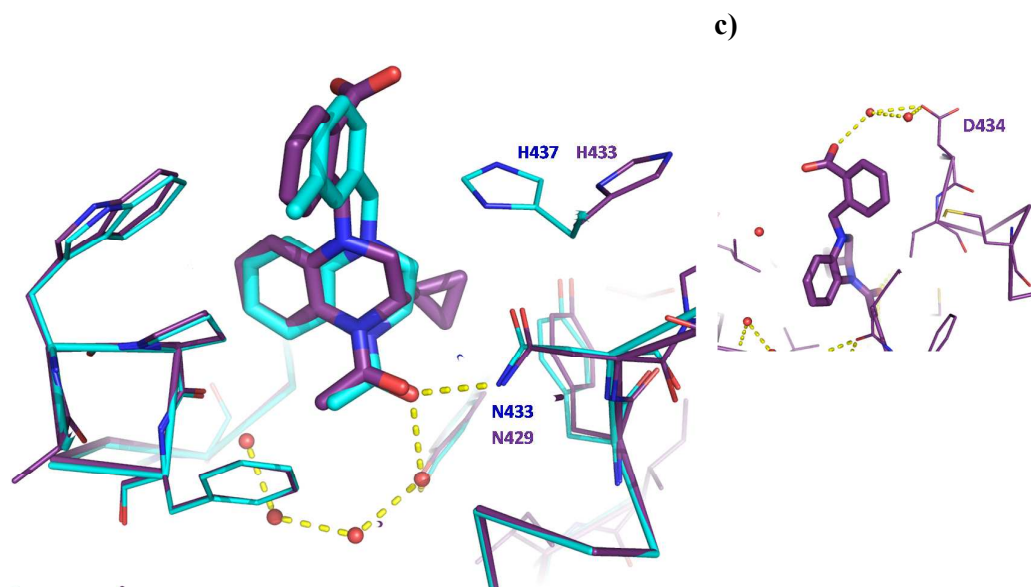


Figure 5 a) X-ray crystal structure of **28c** (purple, PDB code:6FFE) bound to BRD2 BD2 (purple), overlaid with **13** (cyan) bound to BRD4 BD2 (cyan); b) View looking down into the KAc pocket with surface of BRD2 BD2 of **28c** complex shown in grey; bound **28c** (purple) and **13** (cyan); c). Hydrogen bonding of acid of **28c** with D434 shown as yellow dashed lines.

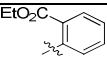
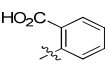
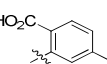
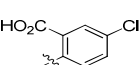
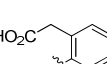
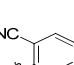
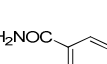
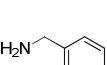
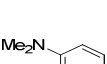
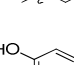

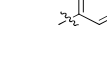
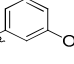
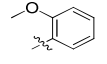
An X-ray structure of **28c** bound to BRD2 BD2 was obtained and compared to that of **13** (Figure 5a). The larger 2-cPr group of **28c** reduces the tetrahydroquinoxaline ring pucker, flattening it and pushing the core closer to the opposite edge of the KAc pocket, which is smaller in BD1 due to the larger I146. Although **28c** was tested as the racemate, only the (*S*)-enantiomer was observed bound to the protein (as also seen with **10**⁶²). The acid of **28c** forms a through-water interaction with D434, though in BRD4 BD2 this residue is a glutamic acid and so may be unable to form this interaction. As such, the selectivity gain from this interaction may be minimal (Figure 5c). The BD2-specific His causes the aryl to adopt a vertical alignment on the WPF shelf, with better contact against W370 of the WPF stack. This subtle cooperativity between the 2-substituent and the WPF shelf-binding group

1
2
3 rationalizes the non-additive elements of the initial SAR, such as the lower potency of 2-
4 methyl *m*-tolyl analogue **26a** compared to **12** and **13**.
5

6
7 With these encouraging results in hand, further substitution of the aryl moiety was
8 investigated with the 2-cyclopropyl group in place (Table 2). The ethyl ester of **28c** (**27c**)
9 displayed similar BD2 potency but increased BD1 potency, indicating that a polar or charged
10 group at C2 confers low BD1 potency. Combination of the tolyl and benzoic acid
11 functionalities (**31**) was detrimental to BD2 potency, while addition of the *p*-Cl functionality
12 seen in **1** (**33**) or a methylene spacer (**35**) had no significant effect on binding. While the
13 nitrile **36** showed poor selectivity and reduced potency, the corresponding amide **37** was
14 pleasingly potent and selective due to a significant reduction in BD1 potency, indicating that
15 the beneficial effect of the *ortho*-substituent is not ionic in nature. Indeed, the basic
16 compounds **38** and **39** showed high BD2 potencies and reasonable selectivity, as did the
17 neutral phenols **40**, **42** and methoxy **43**.
18
19

20
21 Moving the phenol to the *m*-position (**42**) reduced BD2 potency. The benzylic alcohol **44**
22 gave high selectivity and BD2 potency, again with potency reduced on moving substitution to
23 the *m*-position (**45**). Separation and testing of the two enantiomers of **44** (**44a** and **44b**)
24 showed the biological activity is derived solely from one enantiomer, the X-ray structures of
25 similar compounds (not shown) and single enantiomer synthesis support this as the 2-(*S*)
26 enantiomer. Due to concerns about the metabolic stability of the benzylic position, the
27 ethylene glycol derivative **41** was tested, and found to maintain the high potency and
28 selectivity of **44**. Importantly, the inclusion of hydrogen bond donor functionality
29 successfully reduced lipophilicity compared to the cyclopropyl-phenyl analogue **25c**, but the
30 lipophilicity of the highly selective examples **41** and **44** was still high, and further reductions
31 were desired.
32
33
34
35
36
37
38
39
40
41
42
43
44
45
46
47
48
49
50
51
52
53
54
55
56
57
58
59
60

Table 2. Optimization of the WPF shelf binding group.

Cmpd	R	BRD4 FRET pIC ₅₀ ^a		BD2	ChromLogD _{7.4}
		BD1	BD2	Selectivity	
27c		4.9 ± 0.03	6.0 ± 0.08	13	7.2
28c		<4.3 ^b	6.1 ± 0.04	>63	2.2
31		<4.3 ^b	5.6 ± 0.06	20	2.4
33		4.4 ± 0.05	5.9 ± 0.13	32	2.9
35		<4.3 ^b	6.0 ± 0.08	>50	2.4
36		4.6 ± 0.10	5.6 ± 0.01	10	6.0
37		<4.3 ^b	5.9 ± 0.17	>40	3.9
38		4.7 ± 0.03	6.2 ± 0.04	32	2.7
39		4.7 ± 0.07	6.3 ± 0.03	40	7.5
40		4.7 ± 0.18	6.3 ± 0.05	40	5.2
41		4.6 ± 0.07	6.5 ± 0.06	79	4.9
42		4.8 ± 0.12	6.2 ± 0.08	25	4.9
43		4.8 ± 0.07	6.4 ± 0.08	40	6.9
(±)-44		4.5 ± 0.10	6.3 ± 0.08	63	4.9

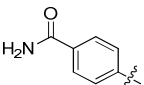
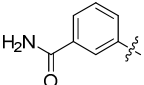
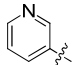
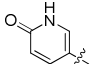
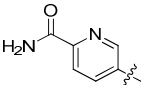
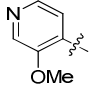
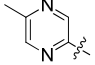
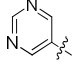
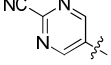
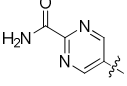
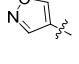
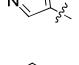
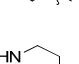
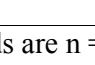
44a		4.8 ± 0.06	6.7 ± 0.05	79	4.7
44b		<4.3 ^b	<4.3 ^b	-	4.7
45		4.6 ± 0.13	6.1 ± 0.09	32	4.7

a) All compounds are n = 3 or greater. Ranges shown are standard deviations. b) Below assay detection limit (50 μM).

With increased selectivity achieved, attention turned to increasing potency and investigating the effect of substitution at the 6-position, which had been shown to increase potency for **3**. With the shelf binder and 2-substituent set as phenyl and ethyl groups, substitution at the 6-position was explored with the goal of protruding through the ZA channel and establishing π -interactions with the WPF tryptophan (Table 3). We focused on aryls and partially saturated rings, in particular heteroaryls, to further reduce lipophilicity and improve the developability profile.⁷¹⁻⁷²

Table 3. Optimization of the 6-aryl substituent.

Cmpd	R	BRD4 FRET pIC ₅₀ ^a		BD2	ChromLogD _{7.4}
		BD1	BD2	Selectivity	
25b	H	5.0 ± 0.15	6.2 ± 0.03	16	6.5
46	Br	5.6 ± 0.10	6.5 ± 0.02	8	7.4

47	Ph	5.8 ± 0.16	6.6 ± 0.14	6	7.9
48		6.4 ± 0.18	7.3 ± 0.14	8	4.4
49		6.3 ± 0.11	7.2 ± 0.12	8	4.7
50		5.8 ± 0.13	7.0 ± 0.17	16	5.6
51		6.1 ± 0.15	7.1 ± 0.07	10	3.5
52		6.2 ± 0.07	7.2 ± 0.08	10	4.5
53		5.3 ± 0.16	6.3 ± 0.18	10	5.4
54		5.7 ± 0.11	6.9 ± 0.07	16	6.1
55		5.5 ± 0.14	6.8 ± 0.19	20	4.9
56		6.6 ± 0.25	7.0 ± 0.17	3	6.3
57		5.7 ± 0.05	7.0 ± 0.05	20	3.6
58		5.8 ± 0.06	6.9 ± 0.03	13	5.9
59		6.4 ± 0.04	7.3 ± 0.06	8	4.2
60		5.8 ± 0.07	6.8 ± 0.13	10	6.5
62		5.5 ± 0.10	6.8 ± 0.12	20	2.8

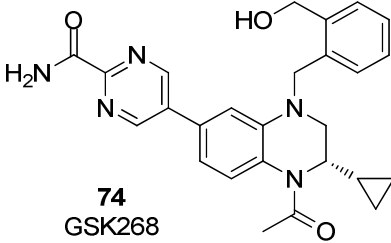
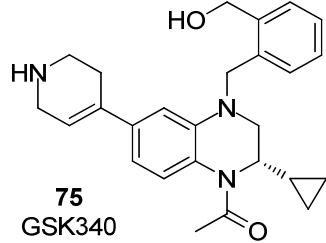
a) All compounds are n = 3 or greater. Ranges shown are standard deviations.

Introduction of a bromide at the 6-position (**46**) increased potency at both bromodomains compared to **25b**, though more so at BD1. The phenyl analogue **47** was less selective and highly lipophilic. With the *para*-position believed to be solvent exposed, polar groups were incorporated here to reduce unfavorable interactions with solvent and reduce lipophilicity. Primary amides **48** and **49** gave a considerable improvement in potency to nanomolar levels, with a concomitant large drop in ChromLogD. Pyridine **50** maintained high potency but regained some BD2 selectivity compared to the phenyl **47**, as such our attention turned to heterocycles. Pyridone **51** showed a marginal drop in selectivity compared to **47**, though lipophilicity was significantly reduced. Combination of the pyridine and amide functionalities gave **52**, which maintained the BD2 potency of **48** and selectivity of **50**. *o*-Substitution (**53**) was detrimental, possibly due to disruption of the water network at the base of the ZA channel or unfavorable increase of the dihedral angle between the core and 6-substituent. It was thought that the lone pair of pyridines **50-52** may either interact with the water network at the base of the ZA channel or point upwards into solvent, reducing unfavorable interactions with aqueous solvent. With this in mind, pyrazine **54** and pyrimidine **55** were tested and found to improve selectivity compared to **50**, though with reduced BD2 potency. The pyrimidine **55** showed better selectivity and was further examined. Introduction of a nitrile substituent (**56**) boosted potency but almost completely abolished selectivity, whereas conversion of **56** to the primary amide **57** re-established selectivity with BD2 potency maintained. The reasons for this dramatic effect are unclear, though several residues beyond the ZA channel differ between BD1 and BD2 and the highly directional lone pair of nitrile **56** may be making a BD1-specific interaction. 5-Membered heterocycles (**58** and **59**) were potent and polar but less selective compared to 6-membered variants. The partially saturated analogues **60** and **62** broadly maintained potency compared to the aryls, with

tetrahydropyridine **62** also being reasonably selective and exhibiting reduced ChromLogD_{7.4} due to the introduction of a basic center.

With good potency, selectivity and ChromLogD_{7.4} profiles, the amidopyrimidine group of **57** and the tetrahydropyridine group of **62** were combined with the previously identified (*S*)-2-cyclopropyl and *ortho*-CH₂OH substituents. After synthesis as single enantiomers (Scheme 5), the resulting compounds **74** and **75** were profiled in biochemical, physicochemical and cellular assays (Table 4).

Table 4. Extended profiles of lead compounds **74** and **75**.^a

 <p>74 GSK268</p>	 <p>75 GSK340</p>	
	GSK268, 74	GSK340, 75
BRD4 BD1/BD2 FRET pIC₅₀ (xSel)	5.7 ± 0.11 / 7.3 ± 0.21 (x40)	5.5 ± 0.13 / 7.2 ± 0.07 (x50)
BRD2 BD1/BD2 FRET pIC₅₀ (xSel)	5.8 ± 0.09 / 7.0 ± 0.10 (x16)	5.6 ± 0.20 / 6.5 ± 0.06 (x8)
BRD3 BD1/BD2 FRET pIC₅₀ (xSel)	6.1 ± 0.17 / 7.5 ± 0.11 (x25)	5.9 ± 0.11 / 7.3 ± 0.10 (x25)

BRDT BD1/BD2 FRET pIC₅₀ (xSel)	6.3 ± 0.10 / 7.0 ±	5.8 ± 0.11 / 6.7 ±
	0.03 (x5)	0.05 (x8)
BRPF1 FRET pIC₅₀	<4	4.7 ± 0.10
Rat Hepatocyte Cl_i (mL/min/g liver)	22.9	8.7
Human Hepatocyte Cl_i (mL/min/g liver)	1.6	1.8
ChromLogD_{7.4}	3.0	2.3
Artificial Membrane Permeability (nm/s)	135	110
CLND Aqueous Solubility (μM)	87	418
FaSSIF Solubility (μg/mL)	18	386
hPBMc LPS-induced MCP-1 Release		
pIC₅₀	7.2 ± 0.23 (n=6)	7.4 ± 0.19 (n=6)
hWB LPS-induced MCP-1 Release pIC₅₀	6.3 ± 0.15 (n=4)	6.0 ± 0.04 (n=4)

a) pIC₅₀ data are n=3 or greater. Ranges shown are standard deviations. The human biological samples were sourced ethically and their research use was in accord with the terms of the informed consents.

Whilst both **74** and **75** showed good BRD4 BD2 potency, tetrahydropyridine **75** was marginally more selective than amidopyrimidine **74** at BRD4. Across the BET family selectivity was lower for both examples, with high potency and reasonable selectivity for BRD3 BD2 but reduced affinity and selectivity for BRD2 and BRDT. This is in contrast to **7**, which exhibits significantly higher domain selectivity at BRD3 compared to BRD2, **4** and **T**. The lower selectivity at BRD2 and BRD3 may be due to subtle changes in the shape of the KAc binding site and WPF shelf, caused by minor residue differences in the ZA and BC loops. BRDT is expressed only in the testes and ovaries⁸ and so is of lesser relevance to cellular phenotype studies. Regardless, in our hands **74** and **75** exhibit improved BD2

potency and selectivity compared to **7** (Table 1), provide an alternative chemotype of BD2-selective BET inhibitors, and offer insights into the rational design of BD2-selective BET inhibitors.

The ChromLogD_{7.4} and artificial membrane permeability (AMP) of both compounds were good, though **75** was significantly more soluble in both thermodynamic and kinetic solubility assays. **74** exhibited high and moderate clearance in rat and human hepatocytes respectively, while for **75** *in vitro* clearance was improved, though still high in rat, and similar to **74** in human. The generally high *in vitro* clearance likely limits the use of **74** and **75** to *in vitro* experiments. Both compounds were cell permeable and active in inhibiting MCP-1 release from human peripheral blood mononuclear cells (PBMCs) and whole blood (hWB) stimulated with lipopolysaccharide (LPS), consistent with reported effects of BET bromodomain inhibition.⁵² The level of human whole blood inhibition is noteworthy as it exceeds the biochemical and biophysical BD1 potencies that have been observed for both **74** and **75**. The decreased potency in hWB compared to the FRET and PBMC potency can be attributed to plasma protein binding, and is of a typical magnitude for these assays. Taking plasma protein binding into account, these data offer good evidence to suggest that inhibition of the BD2 domain is sufficient to drive this response. The opposite enantiomers (**R**)-**74** and (**R**)-**75** showed significantly reduced binding at both bromodomains (see Supporting Information). Binding to BRD4 BD1 and BD2 was also confirmed by surface plasmon resonance (SPR), which showed good correlation with FRET potencies (see Supporting Information).

X-ray crystal structures of **74** and **75** bound to BRD2 BD2 were obtained and showed very similar binding (Figure 6). As expected, the 6-substituent occupies the ZA channel and packs against the WPF motif, making π -interactions with W370, while the primary amide of **74** and the tetrahydropyridine nitrogen of **75** interact with the water network at the exit of the ZA

channel. The benzylic alcohol is capable of forming a hydrogen bond to the BD2 conserved H433, in addition to solvent. The lack of this interaction in the X-ray structure of **74** indicates this may be a relatively weak interaction.

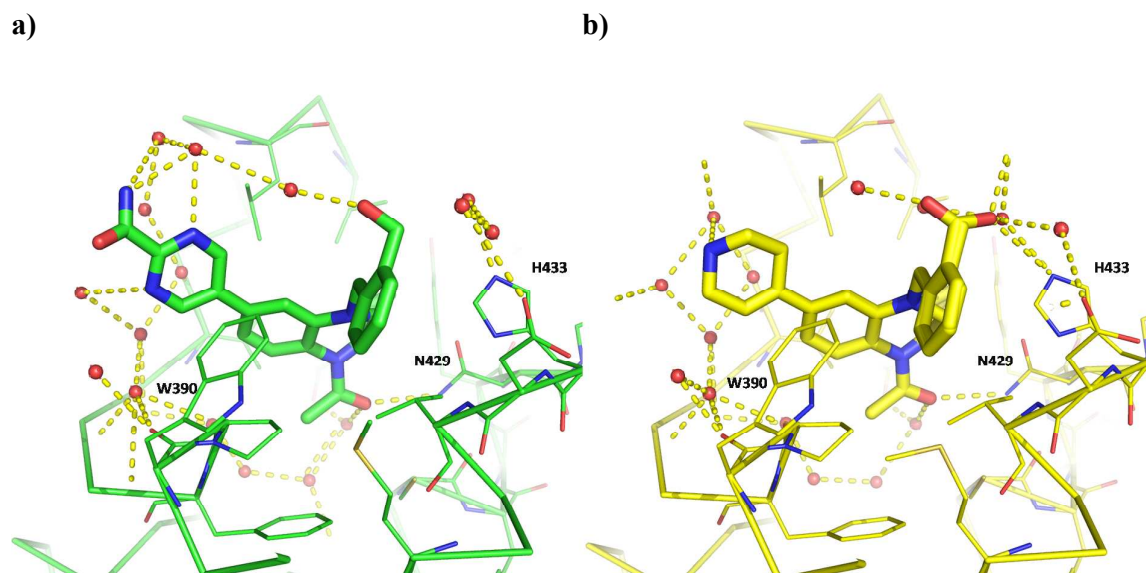


Figure 6. X-ray structure of **a)** **74** (green, PDB code:6FFF) bound to BRD2 BD2 and **b)** an overlay of the two binding modes of **75** (yellow, PDB code:6FFG) found in the crystal structure with BRD2 BD2. Water molecules are shown as red spheres and hydrogen bonds as yellow lines. Key residues are highlighted.

75 was screened against a panel of 35 bromodomains using the DiscoverRx BROMOScan™ assay platform (Figure 7, Table 5).⁷³ The screen showed low-nanomolar potency at each of the BET BD2 domains and good selectivity against BD1, particularly BRD4 where over 220-fold selectivity was recorded. Domain-selectivity was lesser against the other BET BRDs, particularly BRD2 and BRD3, as seen in the FRET assays. Selectivity over non-BET bromodomains was excellent, with the only significant interaction being bromodomain and PHD finger-containing protein 1 (BRPF1), with a ~360-fold window of selectivity compared

to BRD4 BD2. A pIC_{50} of 4.7 (316-fold selectivity) was obtained when **75** was screened in a BRPF1 FRET assay (Table 4). As has been reported previously for BET inhibitors,⁴⁵ the BromoSCAN assay appeared more sensitive than the FRET assays, differences in the selectivity ratios may be attributed to differences in the protein constructs utilized, and inherent differences between pIC_{50} and K_d measurements.

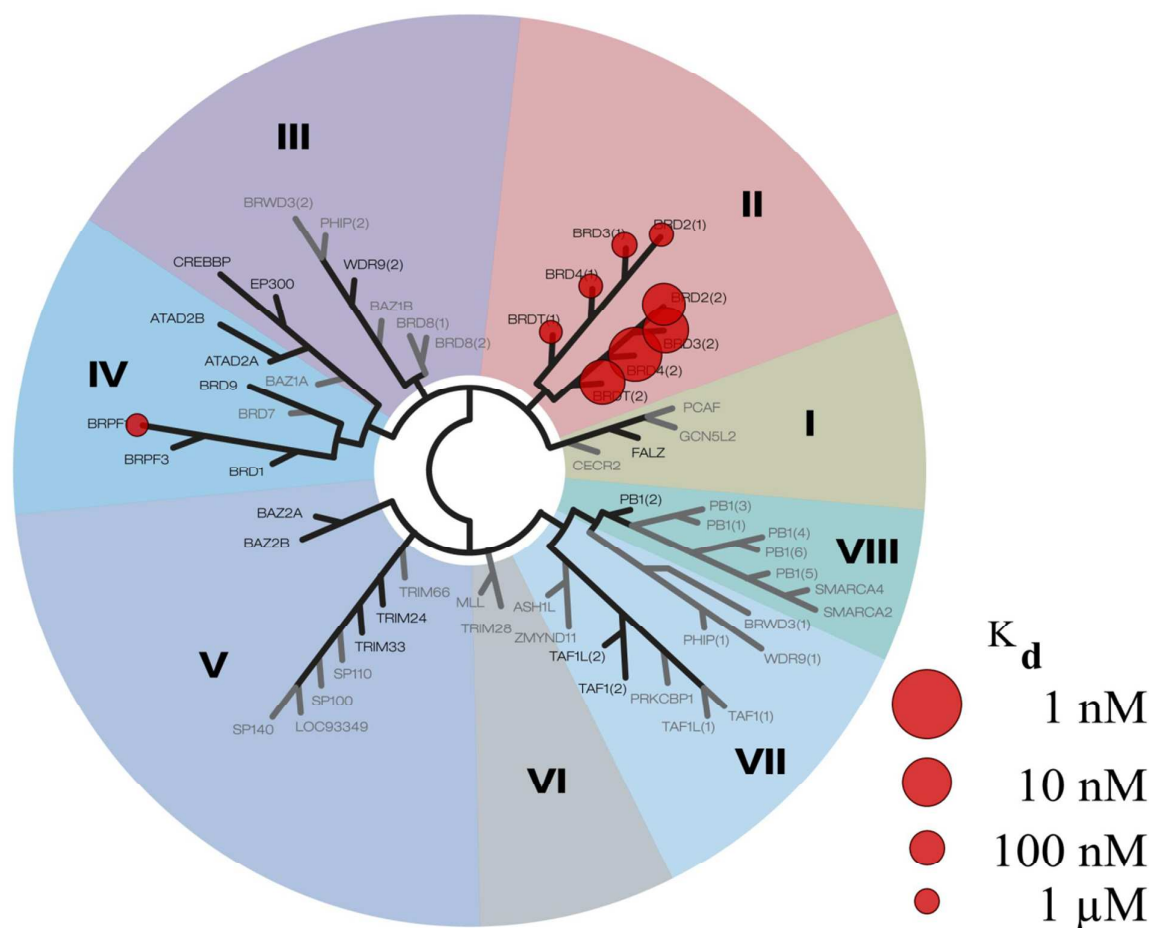


Figure 7. DiscoverX BROMOscan™ bromodomain cross-screen of **75**, showing K_d as circles. Targets with activity <3000 nM are shown. Targets with grayed out names were not screened.

Table 5. DiscoverX BROMOscan™ pK _D values for 75 .	
Target	pK _D
BRD4 BD1 / BD2 (xSel)	5.82 / 8.18 (x229)
BRD2 BD1 / BD2 (xSel)	5.89 / 7.49 (x40)
BRD3 BD1 / BD2 (xSel)	6.04 / 7.72 (x48)
BRDT BD1 / BD2 (xSel)	5.72 / 7.68 (x91)
BRPF1 (xSel vs BRD4 BD2)	5.62 (x363)
TAF1(2)	4.82
WRD9(2)	4.82
ATAD2A/B, BAZ2A/B, BRD1, BRD7, BRD8, BRD9, BRPF3, CECR2, CREBBP, EP300, FALZ, GCN5L2, PBRM1(2/5), PCAF, SMARCA2/4, TAF1L(2), TRIM24(Bromo/PHD), TRIM33(Bromo/PHD),	< 4.52

To further probe the functional cellular effects of BD2-selective inhibition, selected compounds with BD2 selectivity >30-fold were profiled in LPS-stimulated human PBMCs (Table 6). Compounds inhibited the release of the proinflammatory cytokine MCP-1 with pIC₅₀ values significantly higher than the observed BRD4 BD1 potencies, and a general correlation with BRD4 BD2 activity. Notably, **35** and **28c** exhibited MCP-1 inhibition with no detectable BRD4 BD1 activity. These data are indicative of BD2-domain-driven pharmacology and show that BD2-selective BET inhibitors are able to modulate aspects of an immuno-inflammatory response in human cells.

Table 6. Biochemical FRET potency and cellular activity for BD2-selective compounds.			
Compound	BRD4 FRET pIC ₅₀ ^a	BD2 Selectivity (Fold)	PBMC LPS

Number	BD1	BD2		MCP-1 pIC ₅₀
12	4.8 ± 0.16	6.3 ± 0.25	32	5.9 ± 0.22
13	4.8 ± 0.14	6.3 ± 0.54	32	5.5 ± 0.16
25c	4.7 ± 0.07	6.2 ± 0.05	32	5.5 ± 0.21
28b	4.5 ± 0.17	6.1 ± 0.07	40	6.0 ± 0.14
28c	<4.3 ^b	6.1 ± 0.04	63	5.6 ± 0.33
33	4.4 ± 0.05	5.9 ± 0.13	32	4.9 ± 0.07
35	<4.3 ^b	6.0 ± 0.08	50	5.9 ± 0.04
39	4.7 ± 0.07	6.3 ± 0.03	40	5.8 ± 0.1
40	4.7 ± 0.18	6.3 ± 0.05	40	5.9 ± 0.07
43	4.8 ± 0.07	6.4 ± 0.08	40	5.7 ± 0.04
44a	4.8 ± 0.06	6.7 ± 0.05	79	6.0 ± 0.23
45	4.6 ± 0.13	6.1 ± 0.09	32	6.2 ± 0.08
74	5.7 ± 0.11	7.3 ± 0.21	40	7.2 ± 0.23
75	5.5 ± 0.13	7.2 ± 0.07	50	7.4 ± 0.19

Ranges shown are standard deviations. The human biological samples were sourced ethically and their research use was in accord with the terms of the informed consents. *a*) All compounds are n = 2 or greater. *b*) Below assay detection limit (50 μM).

CONCLUSIONS

We have designed and synthesized a series of BD2-selective BET inhibitors with a tetrahydroquinoxaline template. Optimization afforded compounds with high BRD4 BD2 potency, significant selectivity over the BD1 bromodomains, excellent selectivity over all other bromodomains tested and good physicochemical properties. Compound **75** (GSK340) showed nanomolar BRD4 BD2 potency and 50-fold selectivity over BRD4 BD1. **75** is

soluble, permeable and inhibited release of the MCP-1 cytokine in human PBMCs and whole blood. It is therefore suitable for use as an *in vitro* tool molecule. The identification of selective compounds and the biochemical origins of domain selectivity will allow investigation into the biological role of the BD2 domains. This work will also aid the design of further tools with increased selectivity, to unambiguously differentiate the biology of individual domains and determine whether domain selective BET inhibitors are of therapeutic utility.

EXPERIMENTAL

General Experimental Information

Unless otherwise stated, all reactions were carried out under an atmosphere of nitrogen in heat or oven dried glassware and anhydrous solvent. Solvents and reagents were purchased from commercial suppliers and used as received. Reactions were monitored by thin layer chromatography (TLC) or liquid chromatography-mass spectrometry (LC-MS). TLC was carried out on glass or aluminium-backed 60 silica plates coated with UV₂₅₄ fluorescent indicator. Spots were visualized using UV light (254 or 365 nm) or alkaline KMnO₄ solution, followed by gentle heating. LCMS analysis was carried out on a Waters Acquity UPLC instrument equipped with a BEH column (50 mm x 2.1 mm, 1.7 μ m packing diameter) and Waters micromass ZQ MS using alternate-scan positive and negative electrospray. Analytes were detected as a summed UV wavelength of 210 – 350 nm. Flash column chromatography was carried out using Biotage SP4 or Isolera One apparatus with SNAP silica cartridges. Mass directed automatic purification (MDAP) was carried out using a Waters ZQ MS using alternate-scan positive and negative electrospray and a summed UV wavelength of 210 – 350 nm. NMR spectra were recorded at ambient temperature (unless otherwise stated) using standard pulse methods on any of the following spectrometers and signal frequencies: Bruker

AV-400 (^1H = 400 MHz, ^{13}C = 101 MHz), Bruker AV-600 (^1H = 600 MHz, ^{13}C = 150 MHz), Bruker DPX-250 spectrometer at 250 MHz, Varian INOVA spectrometer at 300 MHz. Chemical shifts are referenced to trimethylsilane (TMS) or the residual solvent peak, and are reported in ppm. Coupling constants are quoted to the nearest 0.1 Hz and multiplicities are given by the following abbreviations and combinations thereof: s (singlet), δ (doublet), t (triplet), q (quartet), quin (quintet), sxt (sextet), m (multiplet), br. (broad). IR spectra were obtained on a Perkin Elmer Spectrum 1 machine. Optical rotation of chiral products was measured using a Jasco P1030 polarimeter. Melting point analysis was carried out using a Stuart SMP40 melting point apparatus. Liquid chromatography high resolution mass spectra (HRMS) were recorded on a Micromass Q-ToF Ultima hybrid quadrupole time-of-flight mass spectrometer, with analytes separated on an Agilent 1100 Liquid Chromatograph equipped with a Phenomenex Luna C18(2) reversed phase column (100 mm x 2.1 mm, 3 μm packing diameter). Purity of synthesized compounds was determined by LCMS analysis. All compounds for biological testing were >95% pure.

(S)-7-Chloro-3-cyclopropyl-3,4-dihydroquinoxalin-2(1H)-one (64). (S)-2-Amino-2-cyclopropylacetic acid (**S**)-**15c** (230 mg, 2.00 mmol), 2-bromo-5-chloroaniline **63** (206 mg, 1.00 mmol), CuCl (4.95 mg, 0.05 mmol), DMEDA (22 μL , 0.20 mmol) and DBU (301 μL , 2.00 mmol) were placed in an oven-dried microwave tube which was sealed and placed under N_2 . Anhydrous degassed DMSO (3.5 mL) was added and the reaction mixture was heated to 110 $^\circ\text{C}$ for 20 h. The reaction mixture was cooled, diluted with EtOAc (10 mL) and filtered through Celite. The filtrate was washed with H_2O (2 x 5 mL) and the combined aqueous phases extracted with CHCl_3 (2 x 5 mL). The combined organics were dried through a hydrophobic frit and evaporated *in vacuo*. Purification by silica chromatography (0-100% EtOAc/cyclohexane) afforded the title compound **64** (162 mg, 73%) as an off-white oil which solidified on standing.

LCMS (High pH, ES⁺): t_R = 0.86 min, No mass ion detected, (85% purity). ¹H NMR (400 MHz, CDCl₃): δ 0.21 - 0.33 (m, 1 H), 0.50 - 0.65 (m, 2 H), 0.67 - 0.78 (m, 1 H), 1.16 - 1.30 (m, 1 H), 3.16 (d, J = 8.8 Hz, 1 H), 4.04 (br. s., 1 H), 6.63 (d, J = 8.5 Hz, 1 H), 6.72 (d, J = 2.1 Hz, 1 H), 6.85 (dd, J = 8.5, 2.1 Hz, 1 H), 8.03 (br. s., 1 H). ¹³C NMR (101 MHz, CDCl₃): δ 2.5, 3.2, 14.0, 61.2, 114.9, 115.1, 123.5, 124.0, 126.1, 131.8, 167.5. M.pt.: 165-168 °C. $[\alpha_D]^{25\text{ }^\circ\text{C}} = -4$ (c = 1, CDCl₃).

(S)-6-Chloro-2-cyclopropyl-1,2,3,4-tetrahydroquinoxaline (65). To a solution of **64** (50 mg, 0.23 mmol) in THF (1.5 mL) under N₂ at rt was added 1 M BH₃.THF in THF (674 μ L, 0.67 mmol) dropwise. The reaction was heated to 50 °C for 3 h, then cooled to rt, quenched with MeOH (1 mL) and 1 M HCl (1 mL) and stirred for 30 min. The mixture was basified with 1 M NaOH and extracted with EtOAc (3 x 20 mL). The combined organics were dried and evaporated to dryness. Purification by silica chromatography (0-40% EtOAc/cyclohexane) afforded the title compound **65** (37 mg, 79%) as a white solid. LCMS (High pH, ES⁺): t_R = 1.11 min, $[M+H]^+$ 209.3, (93% pure). ¹H NMR (400 MHz, CDCl₃): δ 0.25 - 0.37 (m, 2 H), 0.51 - 0.64 (m, 2 H), 0.81 - 0.93 (m, 1 H), 2.48 - 2.56 (m, 1 H), 3.26 (dd, J = 10.8, 8.1 Hz, 1 H), 3.45 (dd, J = 10.8, 3.2 Hz, 1 H), 3.75 (br. s., 1 H), 3.84 (br. s., 1 H), 6.42 (d, J = 8.3 Hz, 1 H), 6.47 (d, J = 2.2 Hz, 1 H), 6.53 (dd, J = 8.3, 2.2 Hz, 1 H). ¹³C NMR (101 MHz, CDCl₃): δ 2.0, 2.8, 14.5, 46.4, 55.8, 113.6, 114.7, 118.0, 122.9, 132.0, 134.3. ν_{max} (neat): 3381, 3078, 3003, 2821, 1602, 1508, 1461, 1349, 1307, 1269, 1250, 1137, 1122, 1086, 1017, 957, 845, 795, 705 cm⁻¹. M.pt.: 145-147 °C. $[\alpha_D]^{25\text{ }^\circ\text{C}} = -84$ (c = 1.0, CDCl₃).

(S)-2-Cyclopropyl-1,2,3,4-tetrahydroquinoxaline (66). A mixture of **65** (37 mg, 0.18 mmol) and 10% Pd/C, 50% wt. (8 mg, 0.04 mmol) in EtOH (5 mL) was stirred under an atmosphere of H₂ at rt for 6 h. The reaction mixture was filtered through Celite and the filtrate was evaporated to dryness. The residue was purified by ion exchange chromatography (1 g SCX cartridge, MeOH/2 M NH₃ in MeOH) to afford the title compound **65** (31 mg,

100%) as a brown solid. LCMS (High pH, ES⁺): t_R = 0.83 min, [M+H⁺] 175.2 (100% pure). ¹H NMR (400 MHz, CDCl₃): δ 0.20 - 0.42 (m, 2 H), 0.48 - 0.68 (m, 2 H), 0.78 - 1.01 (m, 1 H), 2.57 (td, *J* = 8.3, 2.9 Hz, 1 H), 3.29 (dd, *J* = 10.5, 8.3 Hz, 1 H), 3.47 (dd, *J* = 10.5, 2.9 Hz, 1 H), 3.58 - 3.90 (m, 1 H), 6.48 - 6.67 (m, 4 H).

(*S*)-*tert*-Butyl 7-chloro-3-cyclopropyl-3,4-dihydroquinoxaline-1(2*H*)-carboxylate (67). To a solution of **65** (840 mg, 4.03 mmol), triethylamine (1122 μL, 8.05 mmol) and DMAP (246 mg, 2.013 mmol) in DCM (16 mL) at 0 °C was added di-*tert*-butyl dicarbonate (966 mg, 4.43 mmol). The reaction mixture was gradually allowed to warm to rt and stirred for 24 h. Further di-*tert*-butyl dicarbonate (200 mg, 0.92 mmol) was added and the reaction was stirred for 24 h. The reaction mixture was diluted with DCM (10 mL) and sat. aq. NaHCO₃ (15 mL). The aqueous layer was extracted with DCM (2 x 20 mL) and the combined organics were dried through a hydrophobic frit and evaporated to dryness. The crude product was purified by silica chromatography (0-35% EtOAc/cyclohexane) to afford the title compound **67** (1060 mg, 3.43 mmol, 85 % yield) as an off-white solid. LCMS (High pH, ES⁺): t_R = 1.43 min, [M+H⁺] 307.3, (98% pure). ¹H NMR (400 MHz, CDCl₃): δ 0.26 - 0.39 (m, 2 H), 0.51 - 0.63 (m, 2 H), 0.74 - 0.91 (m, 1 H), 1.54 (s, 9 H), 2.61 (s, 1 H), 3.18 - 3.33 (m, 1 H), 4.00 - 4.24 (m, 2 H), 6.49 (d, *J* = 8.6 Hz, 1 H), 6.86 (dd, *J* = 8.6, 2.2 Hz, 1 H), 7.55 (br. s., 1 H). ¹³C NMR (101 MHz, CDCl₃): δ 1.8, 2.6, 14.3, 28.3, 46.2, 56.4, 81.3, 114.8, 120.9, 124.2, 124.4, 125.1, 135.4, 153.0. M.pt.: 142-144 °C. ν_{max} (neat): 3368, 2988, 1675, 1560, 1501, 1454, 1401, 1374, 1294, 1237, 1153, 1098, 1077, 1046, 1035, 1018, 984, 869, 860, 804, 766 cm⁻¹. [α_D]^{25 °C} = -65 (c = 1.0, CDCl₃). HRMS: (C₁₆H₂₁ClN₂O₂) [M+H]⁺ requires 309.1364, found [M+H]⁺ 309.1363.

(*S*)-1-(6-Chloro-2-cyclopropyl-3,4-dihydroquinoxalin-1(2*H*)-yl)ethanone (69). To a solution of **67** (1.06 g, 3.43 mmol) in 2-MeTHF (35 mL) at rt stirred under nitrogen was added triethylamine (5.74 mL, 41.2 mmol) and acetic anhydride (3.24 mL, 34.3 mmol). The

reaction mixture was stirred at 90 °C for 18 h. The reaction mixture was cooled, diluted with EtOAc (20 mL) and washed with 1M HCl (3 x 20 mL) and sat. aq. NaHCO₃ (3 x 20 mL). The organic layer was dried through a hydrophobic frit and evaporated to dryness. The residue was dissolved in DCM (3 mL) and trifluoroacetic acid (TFA) (3 mL) was added. The reaction was stirred at rt for 3 h, then evaporated and the residue partitioned between EtOAc (20 mL) and sat. aq. NaHCO₃ solution (20 mL). The aqueous layer was extracted with EtOAc (2 x 20 mL) and the combined organics were dried through a hydrophobic frit and evaporated to dryness. The residue was purified by silica chromatography (0-100% EtOAc/cyclohexane) to afford the title compound **69** (680 mg, 2.71 mmol, 80 % yield) as a white solid. LCMS (High pH, ES⁺): t_R = 1.04 min, [M+H⁺] 251.16, (94% purity). ¹H NMR (400 MHz, CDCl₃): δ 0.29-0.59 (m, 4 H), 0.70-0.88 (m, 1 H), 2.23 (s, 3 H), 3.40 (dd, *J* = 11.5, 4.2 Hz, 1 H), 3.49 (ddd, *J* = 11.5, 4.9, 1.2 Hz, 1 H), 4.08-4.30 (m, 1 H), 4.37 (br. s., 1 H), 6.57-6.65 (m, 2 H), 6.87-7.04 (m, 1 H). ¹³C NMR (101 MHz, CDCl₃): δ 3.8, 4.3, 11.9, 22.8, 45.8, 50.5, 113.3, 116.0, 121.2, 126.5, 131.3, 138.5, 168.9. ν_{max} (neat): 3299, 3004, 2866, 1630, 1603, 1502, 1444, 1380, 1313, 1238, 1227, 1095, 1067, 1023, 874, 849, 788 cm⁻¹. M.pt.: 122-126 °C. [α]_D²⁵ °C = +208 (c = 1.0, CDCl₃). HRMS: (C₁₃H₁₅ClN₂O) [M+H]⁺ requires 251.0946, found [M+H]⁺ 251.0948.

((2-(Bromomethyl)benzyl)oxy)(tert-butyl)dimethylsilane (70). To a solution of (2-(bromomethyl)phenyl)methanol (330 mg, 1.64 mmol) in DCM (7 mL) under N₂ at rt was added 2,6-lutidine (0.38 mL, 3.28 mmol) and *tert*-butyldimethylsilyl trifluoromethanesulfonate (0.57 mL, 2.46 mmol). The reaction mixture was stirred at rt for 1 h, then quenched with H₂O (5 mL) and the aqueous layer extracted with EtOAc (2 x 15 mL). The combined organics were dried, evaporated and the crude product purified by silica chromatography (0-20% EtOAc/cyclohexane) to afford the title compound **70** (490 mg, 95%) as a clear oil. LCMS (High pH, ES⁺): t_R = 1.61 min (100% purity). No mass ion observed. ¹H

NMR (400 MHz, CDCl₃): δ 0.14 (s, 6 H), 0.97 (s, 9H), 4.61 (s, 2 H), 4.89 (s, 2 H), 7.28 (s, 3 H), 7.44 - 7.49 (m, 1 H). Analysis consistent with literature.⁷⁴

(S)-1-(4-(2-(((*tert*-Butyldimethylsilyl)oxy)methyl)benzyl)-6-chloro-2-cyclopropyl-3,4-dihydroquinoxalin-1(2*H*)-yl)ethanone (71). To a solution of **69** (130 mg, 0.518 mmol) in DMF (6 mL) at 0 °C was added sodium hydride (60% wt. in mineral oil, 62 mg, 1.555 mmol), and the reaction was stirred under nitrogen at 0 °C for 5 min. A solution of **70** (204 mg, 0.648 mmol) in DMF (0.6 mL) was added dropwise and the reaction was stirred at 0 °C for 90 min. The reaction mixture was poured into water (30 mL) and extracted with Et₂O (3 x 10 mL). The combined organics were dried through a hydrophobic frit, evaporated to dryness and the residue was purified by silica chromatography (0-20% EtOAc/cyclohexane) to afford the title compound **71** (200 mg, 0.412 mmol, 80%). LCMS (High pH, ES⁺): t_R = 1.73 min, [M+H⁺] 485.4, 487.4, (97% purity). ¹H NMR (400 MHz, CDCl₃) δ 0.10 (s, 6 H), 0.29-0.38 (m, 1 H), 0.40-0.57 (m, 3 H), 0.85-0.93 (m, 1 H), 0.94 (s, 9H), 2.24 (s, 3 H), 3.38 (dd, J = 11.3, 1.0 Hz, 1 H), 3.51 (dd, J = 11.5, 4.7 Hz, 1 H), 4.13-4.34 (m, 1 H), 4.61 (d, J = 4.9 Hz, 2 H), 4.74 (s, 2 H), 6.55 (d, J = 2.2 Hz, 1 H), 6.64 (dd, J = 8.3, 2.2 Hz, 1 H), 6.92-7.06 (m, 1 H), 7.13-7.31 (m, 3 H), 7.42 (dd, J = 7.3, 1.00 Hz, 1 H). ¹³C NMR (101 MHz, CDCl₃) δ -5.2, 4.0, 4.2, 12.5, 18.3, 22.7, 25.9, 51.7, 51.8, 52.9, 63.4, 110.9, 115.6, 121.9, 125.5, 126.3, 127.2, 127.8, 128.1, 132.1, 134.3, 138.4, 140.1, 168.8. ν_{max} (neat): 2956, 2928, 2893, 2855, 1644, 1597, 1511, 1392, 1359, 1337, 1306, 1256, 1094, 1057, 1041, 833, 777, 742 cm⁻¹. M.pt.: 136-139 °C. HRMS: (C₂₇H₃₈ClN₂O₂Si) [M+H]⁺ requires 485.2386, found [M+H]⁺ 485.2400. [α_D]^{25 °C} = +50 (c = 1.0, CDCl₃).

(S)-*tert*-Butyl 4-(1-acetyl-4-(2-(((*tert*-butyldimethylsilyl)oxy)methyl)benzyl)-2-cyclopropyl-1,2,3,4-tetrahydroquinoxalin-6-yl)-5,6-dihydropyridine-1(2*H*)-carboxylate (73). A solution of **71** (29 mg, 0.060 mmol), (1-(*tert*-butoxycarbonyl)-1,2,3,6-tetrahydropyridin-4-yl)boronic acid (37 mg, 0.120 mmol), BrettPhos Pd G3 (5 mg, 5.98

μmol) and cesium carbonate (58 mg, 0.179 mmol) in degassed DME (0.6 mL) was sealed in a microwave vial, placed under nitrogen and heated in a Biotage Initiator microwave to 110 °C for 2 h. The reaction mixture was filtered through Celite and evaporated to dryness. The residue was purified by silica chromatography (0-35% EtOAc/cyclohexane) and High pH MDAP to give the title compound **73** (26 mg, 0.041 mmol, 69%) as an off-white gum. LCMS (High pH, ES⁺): t_R = 1.76 min, [M+H]⁺ 632.5, (93% pure). ¹H NMR (400 MHz, CDCl₃) δ 0.10 (s, 6 H), 0.29 - 0.37 (m, 1 H), 0.41 - 0.55 (m, 3 H), 0.89 - 0.98 (m, 1 H), 0.93 (s, 9 H), 1.46 (s, 9 H), 2.27 (s, 3 H), 2.33 - 2.40 (m, 2 H), 3.39 (dd, *J* = 11.2, 1.0 Hz, 1 H), 3.49 - 3.57 (m, 3 H), 3.98 (q, *J* = 2.4 Hz, 2 H), 4.17 - 4.30 (m, 1 H), 4.63 (s, 2 H), 4.76 (s, 2 H), 5.79 - 5.88 (m, 1 H), 6.56 (d, *J* = 1.7 Hz, 1 H), 6.69 (dd, *J* = 8.3, 1.7 Hz, 1 H), 6.98 - 7.10 (m, 1 H), 7.17 - 7.30 (m, 3 H), 7.42 (d, *J* = 7.6 Hz, 1 H). ¹³C NMR (101 MHz, CDCl₃) δ -5.2, 4.0, 4.1, 12.6, 18.3, 22.8, 25.9, 27.4, 28.5, 40.9, 43.6, 51.8, 52.2, 53.2, 63.4, 79.6, 107.7, 112.7, 120.5, 122.7, 125.3, 125.7, 127.1, 127.7, 127.9, 135.0, 135.3, 138.3, 139.1, 139.1, 154.8, 168.8. ν_{max} (neat): 2929, 2856, 1692, 1651, 1516, 1365, 1336, 1291, 1240, 1168, 1113, 1063, 956, 835, 775, 732, 666 cm⁻¹. HRMS: (C₃₇H₅₃N₃O₄Si) [M+H]⁺ requires 632.3878, found [M+H]⁺ 632.3884. [α_D]^{22 °C} = +110 (c = 0.1, MeOH).

(S)-1-(2-Cyclopropyl-4-(2-(hydroxymethyl)benzyl)-6-(1,2,3,6-tetrahydropyridin-4-yl)-3,4-dihydroquinoxalin-1(2H)-yl)ethanone (75). To a solution of **73** (26 mg, 0.041 mmol) in MeOH (0.4 mL) was added HCl, 1M in diethyl ether (0.8 mL, 0.823 mmol), and the reaction was stirred at rt for 6 h. The reaction was purified by ion exchange chromatography (sulphonic acid (SCX), 1 g, sequential solvents methanol, 2M ammonia/methanol), appropriate fractions were evaporated to dryness. The product was further purified by silica chromatography (0-100% 3:1 EtOAc:EtOH/cyclohexane). The appropriate fractions were evaporated to dryness. The product was further purified by Formic MDAP, the appropriate fractions were evaporated to dryness. The product was desalted using ion exchange

chromatography (sulphonic acid (SCX), 500 mg, sequential solvents methanol, 2 M ammonia/methanol), affording the title compound **75** (8 mg, 0.019 mmol, 47%). LCMS (ES⁺): t_R = 0.64 min, [M+H]⁺ 418.2, (97% purity). ¹H NMR (400 MHz, CDCl₃) δ 0.27 - 0.36 (m, 1 H), 0.39 - 0.55 (m, 3 H), 0.86 - 0.98 (m, 1 H), 2.26 (s, 3 H), 2.30 - 2.36 (m, 2 H), 3.03 (t, J = 5.6 Hz, 2 H), 3.33 (dd, J = 11.1, 1.5 Hz, 1 H), 3.44 - 3.47 (m, 2 H), 3.50 (dd, J = 11.1, 5.0 Hz, 1 H), 4.16 - 4.31 (m, 1 H), 4.68 (s, 2 H), 4.76 (s, 2 H), 5.95 - 6.00 (m, 1 H), 6.68 (d, J = 1.7 Hz, 1 H), 6.74 (dd, J = 8.1, 1.7 Hz, 1 H), 6.98 - 7.11 (m, 1 H), 7.22 - 7.33 (m, 3 H), 7.41 (d, J = 6.6 Hz, 1 H). NH and OH not observed. ¹³C NMR (101 MHz, CDCl₃) δ 3.9, 4.1, 12.7, 22.8, 27.5, 43.1, 45.2, 52.1, 52.4 (broad), 53.3, 63.0, 108.1, 113.0, 122.8, 122.9, 123.0, 125.3, 126.7, 127.3, 128.1, 128.7, 135.2, 135.8, 138.6, 139.1, 139.6, 168.9. M.pt. 170-173 °C. ν_{\max} (neat): 3343, 2865, 1621, 1518, 1395, 1375, 1314, 1241, 1088, 961, 842, 795, 745 cm⁻¹. HRMS: (C₂₆H₃₁N₃O₂) [M+H]⁺ requires 418.2489, found [M+H]⁺ 418.2491. [α_D]^{22 °C} = +119 (c = 0.1, MeOH).

CLND Solubility

Solubility was determined by precipitation of 10 mM DMSO stock concentration to 5% DMSO pH 7.4 phosphate buffered saline, with quantification by ChemiLuminescent Nitrogen Detection.

FaSSIF solubility

Compounds were dissolved in DMSO at 2.5 mg/mL and then diluted in Fast State Simulated Intestinal Fluid (FaSSIF pH 6.5) at 125 μ g/mL (final DMSO concentration is 5%). After 16h of incubation at 25°C, the suspension was filtered. The concentration of the compound was determined by a fast HPLC gradient. The ratio of the peak areas obtained from the standards and the sample filtrate was used to calculate the solubility of the compound.

ChromLogD_{7.4}

Chromatographic hydrophobicity index (ChiLogD_{7.4}) was determined using fast gradient HPLC, according to literature procedures,⁷⁵⁻⁷⁶ using a Waters Aquity UPLC System, Phenomenex Gemini NX 50x2 mm, 3 μ m HPLC column, 0-100% pH 7.40 ammonium acetate buffer/acetonitrile gradient. Retention time was compared to standards of known pH to derive Chromatographic Hydrophobicity Index (CHI). $\text{ChromLogD} = 0.0857\text{CHI} - 2$.

Artificial membrane permeability

Permeability across a lipid membrane was measured using the published protocol.⁷⁷

Intrinsic Clearance (Ci) Measurements

Experimental Protocol

Intrinsic Clearance (Cli) data was determined by Cypotex UK. Test compound (0.5 μ M) was incubated with cryopreserved hepatocytes in suspension. Samples were removed at 6 time points over the course of a 60 min (rat) or 120 min (human) experiment and test compound is analyzed by LC-MS/MS. Cryopreserved pooled hepatocytes were purchased from a reputable commercial supplier and stored in liquid nitrogen prior to use. Williams E media supplemented with 2 mM L-glutamine and 25 mM HEPES and test compound (final substrate concentration 0.5 μ M; final DMSO concentration 0.25 %) was pre-incubated at 37 °C prior to the addition of a suspension of cryopreserved hepatocytes (final cell density 0.5×10^6 viable cells/mL in Williams E media supplemented with 2 mM L-glutamine and 25 mM HEPES) to initiate the reaction. The final incubation volume was 500 μ L. The reactions were stopped by transferring 50 μ L of incubate to 100 μ L acetonitrile at the appropriate time points. The termination plates were centrifuged at 2500 rpm at 4 °C for 30 min to precipitate the protein. The remaining incubate (200 μ L) was crashed with 400 μ L acetonitrile at the end of the incubation. Following protein precipitation, the sample supernatants were combined in cassettes of up to 4 compounds and analyzed using Cypotex generic LC-MS/MS conditions.

Data Analysis

From a plot of ln peak area ratio (compound peak area/internal standard peak area) against time, the gradient of the line was determined. Subsequently, half-life ($t_{1/2}$) and intrinsic clearance (CL_{int}) were calculated using the equations below:

Elimination rate constant (k) = (- gradient)

$$\text{Half-life } (t_{1/2})(\text{min}) = \frac{0.693}{k}$$

$$\text{Intrinsic clearance } (CL_{int})(\mu\text{L}/\text{min}/\text{million cells}) = \frac{V \times 0.693}{t_{1/2}}$$

where V = Incubation volume (μL)/Number of cells

hWB MCP-1 Assay

Compounds to be tested were diluted in 100% DMSO to give a range of appropriate concentrations at 140x the required final assay concentration, of which 1 μL was added to a 96 well tissue culture plate. 130 μL of human whole blood, collected into sodium heparin anticoagulant, (1 unit/mL final) was added to each well and plates were incubated at 37°C (5% CO₂) for 30 min before the addition of 10 μL of 2.8 $\mu\text{g}/\text{mL}$ LPS (Salmonella Typhosa), diluted in complete RPMI 1640 (final concentration 200ng/mL), to give a total volume of 140 μL per well. After further incubation for 24 h at 37°C, 140 μL of PBS was added to each well. The plates were sealed, shaken for 10 min and then centrifuged (2500rpm x 10 min). 100 μL of the supernatant was removed and MCP-1 levels assayed immediately by immunoassay (MesoScale Discovery technology).

PBMC MCP-1 Assay

Human PBMCs (cryopreserved in 90% serum, 10% DMSO) were thawed and 5 mL warm media per 1 mL cells was added dropwise, and centrifuged at 1600 rpm for 5 min. The supernatant was decanted and the pellet was resuspended in 10 mL pre-warmed assay medium (RPMI-1640, Foetal Calf Serum (50 mL in 500 mL), Penicillin/Streptomycin (5 mL

to 500 mL), L-Glutamine 200 mM (5 mL to 500 mL)). The cells were counted on a CEDEX cell counter and diluted to a final conc. of 0.32×10^6 (40000 cells)/mL. Compounds to be tested were diluted in 100% DMSO to give a range of appropriate concentrations. 130 μ L of the cell suspension was added to each well of the compound plates containing 0.5 μ L of compound in each well and incubated at 37°C, 5% CO₂ for 30 min. After 30 min 10 μ L of 14 ng/mL LPS (Salmonella Typhosa), diluted in complete RPMI 1640, was added to each well (final = 1ng/mL) (total volume per well of 140.5 μ L). The plates were incubated at 37 degrees, 5% CO₂ for 24 hours. 20 μ L of supernatant was transferred to an MCP-1 coated 96 well MSD plate and incubated for 1-2 hr on a plate shaker. 20 μ L 1X sulfo-TAG antibody (final conc 1 μ g) was added to each well and the plates were incubated for 1-2 hr at room temperature whilst shaking. The plates were washed 3 times using a plate washer and 150 μ L MSD read buffer P/T (2X) was added to the plate. The plates were read on the MSD reader to determine MCP-1 levels by immunoassay (MesoScale Discovery technology).

TR-FRET Assays

BET proteins were produced using published protocols.⁴⁷ Compounds were screened against either 6H-Thr BRD4 (1-477) (Y390A) (BRD4 BD2 mutation to monitor compound binding to BD1) or 6H-Thr BRD4 (1-477) (Y97A) (BRD4 BD1 mutation to monitor compound binding to BD2) in a dose-response format in a TR-FRET assay measuring competition between test compound and an AlexaFluor647 derivative of **2**. Compounds were titrated from 10 mM in 100% DMSO and 50 nL transferred to a low volume black 384 well micro titre plate using a Labcyte Echo 555. A Thermo Scientific Multidrop Combi was used to dispense 5 μ L of 20 nM protein in an assay buffer of 50 mM HEPES, 150 mM NaCl, 5% glycerol, 1 mM DTT and 1 mM CHAPS, pH 7.4, and in the presence of 100 nM fluorescent ligand (~K_d concentration for the interaction between BRD4 BD1 and ligand). After equilibrating for 30 min in the dark at rt, the bromodomain protein: fluorescent ligand interaction was detected

using TR-FRET following a 5 μ L addition of 3 nM europium chelate labelled anti-6His antibody (Perkin Elmer, W1024, AD0111) in assay buffer. Time resolved fluorescence (TRF) was then detected on a TRF laser equipped Perkin Elmer Envision multimode plate reader (excitation = 337 nm; emission 1 = 615 nm; emission 2 = 665 nm; dual wavelength bias dichroic = 400 nm, 630 nm). TR-FRET ratio was calculated using the following equation: Ratio = ((Acceptor fluorescence at 665 nm) / (Donor fluorescence at 615 nm)) * 1000. TR-FRET ratio data was normalized to high (DMSO) and low (compound control derivative of **2**) controls and IC₅₀ values determined for each of the compounds tested by fitting the fluorescence ratio data to a four parameter model: $y = a + ((b - a) / (1 + (10^x / 10^c)^d))$ where 'a' is the minimum, 'b' is the Hill slope, 'c' is the IC₅₀ and 'd' is the maximum. BRPF1 protein was produced using protocols given in the literature.⁷⁸ Compounds were screened against 6H-Flag-Tev-BRPF1 (622-738) protein in dose-response format in a TR-FRET assay measuring competition between test compound and a synthetic fluorescent ligand. Compounds were titrated from 10 mM in 100% DMSO and 100 nL transferred to a low volume black 384 well micro titre plate using a Labcyte Echo 555. A Thermo Scientific Multidrop Combi was used to dispense 5 μ L of 4 nM BRPF1, 20 nM BRPF2 or 40 nM BRPF3 protein respectively in an assay buffer of 50 mM HEPES, 150 mM NaCl, 5% glycerol, 1mM DTT and 1 mM CHAPS, pH 7.4, and in the presence of the appropriate fluorescent ligand concentration (~K_d concentration for the interaction between protein and ligand). After equilibrating for 30 min in the dark at rt, the bromodomain protein: fluorescent ligand interaction was detected using TR-FRET following a 5 μ L addition of either 3 nM Lanthascreen Elite Tb-anti His antibody (Invitrogen PV5863) for the Alexa 488 ligands, or 3 nM europium chelate labelled anti-6His antibody (Perkin Elmer, W1024, AD0111) for the Alexa 647 ligand, in assay buffer. Time resolved fluorescence energy transfer (TR-FRET) was then detected on a time-resolved fluorescence laser equipped Perkin Elmer Envision

multimode plate reader using the appropriate protocol (excitation = 337 nm; emission 1 Alexa 488 = 495 nm; emission 2 Alexa 488 = 520 nm, emission 1 Alexa 647 = 615 nm; emission 2 Alexa 647 = 665 nm). TR-FRET ratio was calculated using the following equation: Ratio = ((Acceptor fluorescence at 520 or 665 nm) / (Donor fluorescence at 495 or 615 nm)) * 1000. Data were analyzed as for the BRD4 assay.

BROMOscan® Bromodomain Profiling

BROMOscan® bromodomain profiling was provided by DiscoverX Corp. (Fremont, CA, USA, <http://www.discoverx.com>). Determination of the K_d between test compounds and DNA tagged bromodomains was achieved through binding competition against a proprietary reference immobilized ligand.

X-Ray Crystallography

Human BRD4 BD2 Cocrystallisation and Structure determination

BRD4-BD2 ligand complexes were co-crystallized with at least 3:1 excess of compound @10.5mg/ml in 120nl+120nl sitting drops using a 96 well MRC plate with a well solution of Morpheus condition D2 (0.1M morpheus buffer 1, pH 6.5, 30% morpheus EDO_P8K, 0.12M Morpheus alcohol mixture. Crystals were fished out straight from the drop prior to flash freezing in liquid nitrogen. X-ray diffraction data were collected at 100 K on id23eh1 at the European synchrotron radiation facility (ESRF, Grenoble). The data were processed and scaled using MOSFLM⁷⁹ and SCALA within the CCP4 suite of programs.⁸⁰⁻⁸¹ The crystal space group is P22121 with a single molecule in the asymmetric unit. Data collection statistics are given in Table S3. The structures were determined using the coordinates of an isomorphous unliganded protein model, with preliminary refinement carried out using REFMAC5.⁸²⁻⁸³ In all cases, the ligands were clearly visible in the resulting Fo-Fc electron density maps (Table S4). Coot⁸⁴ was used for model building, with refinement completed using autoBUSTER. The statistics for the final models are given in Table S2.

Human BRD2 BD2 Soaked complexes and Structure determination

BRD2 BD2 *apo* crystals were grown in 1uL+1uL streak seeded hanging drops in 15 well plates with a well solution of 30% PEG 300, 0.1M MES buffer pH 6.5 at 20 °C. *Apo* crystals were harvested into a fresh 1.5 uL hanging drop containing 5% DMSO and nominally > 1 mM ligand. Soaked crystals were briefly cryoprotected in well solution with the addition of 10% ethylene glycol prior to plunge freezing in liquid nitrogen. X-ray diffraction data were collected at 100 K on an in house RIGAKU FR-E SUPERBRIGHT/A200 system. The data were processed and scaled using XDS⁸⁵⁻⁸⁶ or MOSFLM and SCALA within the CCP4 suite of programs.⁸¹ The crystal space group is P2₁2₁2 with a single molecule in the asymmetric unit. Data collection statistics are given in Table S3. The structures were determined using the coordinates of an isomorphous unliganded protein model, with preliminary refinement carried out using REFMAC5.⁸²⁻⁸³ In all cases, the ligands were clearly visible in the resulting F_o-F_c electron density maps (Table S3). Coot⁸⁴ was used for model building. The statistics for the final models are given in Table S3.

Assay Interference Compounds

All compounds for biological testing were screened against known assay interference chemotypes by the authors, and using GSK proprietary *in silico* models. No flags were reported except for **40**, which flagged for Mannich reactivity⁸⁷ and so was not investigated further.

ANCILLARY INFORMATION

Supporting Information

Full synthetic procedures and characterization data for all compounds, curves for FRET and MCP-1 data for **74** and **75**, profiles for (**R**)-**74** and (**R**)-**75**, full BROMOscan data for **75**, X-

ray data collection and refinement, SPR data for **74** and **75**, chiral analysis of **75**,
supplementary data (PDF), molecular formula strings (CSV).

This material is available free of charge via the ACS Publications website at
<http://pubs.acs.org>.

PDB ID Codes

The coordinates and structure factors are deposited in the Protein Data Bank as 6FFD, 6FFE,
6FFF and 6FFG. Authors will release the atomic coordinates and experimental data upon article
publication.

AUTHOR INFORMATION

Corresponding Author

*For R.P.L. Email: robert.p.law@gsk.com.

Present Addresses

(A.J.B.W.) School of Chemistry, University of St Andrews, North Haugh, St Andrews, KY16
9ST, U.K.

Author Contributions

The manuscript was written through contributions of all authors. All authors have given
approval to the final version of the manuscript.

Acknowledgements

R.P.L is grateful to GlaxoSmithKline R&D, Stevenage for Ph.D. studentship funding. Chiral
analysis and separation was carried out by Eric Hortense, and HRMS analysis by Bill
Leavens. hWB and PBMC data was generated by Rob Davies and Alexander Phillipou.

Proteins were expressed and purified by Paul Homes and Nathalie Barrett. We also wish to thank Lee Harrison, Christopher Wellaway, Gail Seal, Jon Seal, Alex Preston and Hawa Diallo for helpful discussions throughout the course of this work, and Sean Lynn for assistance with NMR spectra.

Abbreviations

AMP, artificial membrane permeability; ApoA1, Apolipoprotein A1; BD1, first (N-terminal) bromodomain; BD2, second (C-terminal) bromodomain; BET, bromodomain and extra-terminal domain; Boc, *tert*-butoxycarbonyl; BRD, bromodomain-containing protein; BRD2/3/4, bromodomain-containing protein 2/3/4; BRDT, bromodomain, testis-specific; BRPF1, bromodomain and PHD finger-containing protein 1; ChromLogD, chromatographic LogD, CLND, chemoluminescent nitrogen detection; DCM, dichloromethane; DBU, 1,8-diazabicyclo[5.4.0]undec-7-ene; DIPEA, diisopropylethylamine; DMAP, 4-(dimethylamino)pyridine; DME, 1,2-dimethoxyethane; DMEDA, N,N'-Dimethylethylenediamine; DMF, *N,N*-dimethylformamide; DMSO, dimethylsulfoxide; FRET, fluorescence resonance energy transfer; HPLC, high performance liquid chromatography; HRMS, high resolution mass spectra; hWB, human whole blood; IL-6, interleukin 6; Janus kinase/signal transducers and activators of transcription (JAK-STAT); KAc, N-acetyl lysine; LE, ligand efficiency; LPS, lipopolysaccharide; MCP-1, monocyte chemoattractant protein 1; MDAP, mass-directed automatic purification; 2-MeTHF, 2-methyltetrahydrofuran; NMC, NUT midline carcinoma; NUT, nuclear protein in testis; PAFc, polymerase-associated factor complex; PTEF-b, positive transcription elongation factor; TBAF, tetrabutyl ammonium fluoride; TFA, trifluoroacetic acid; THF, tetrahydrofuran; TLC, thin-layer chromatography; WPF, tryptophan-proline-phenylalanine.

Notes

The authors declare the following competing financial interest(s): All authors except R.P.L and A.J.B.W were GlaxoSmithKline full-time employees at the time when this study was performed. All studies involving the use of animals were conducted after review by the GlaxoSmithKline (GSK) Institutional Animal Care and Use Committee and in accordance with the GSK Policy on the Care, Welfare, and Treatment of Laboratory Animals.

REFERENCES

1. Prinjha, R. K.; Witherington, J.; Lee, K. Place your BETs: the therapeutic potential of bromodomains. *Trends Pharmacol. Sci.* **2012**, *33*, 146–153.
2. Belkina, A. C.; Denis, G. V. BET domain co-regulators in obesity, inflammation and cancer. *Nat. Rev. Cancer.* **2012**, *12*, 465–477.
3. Arrowsmith, C. H.; Bountra, C.; Fish, P. V.; Lee, K.; Schapira, M. Epigenetic protein families: a new frontier for drug discovery. *Nat. Rev. Drug. Discov.* **2012**, *11*, 384–400.
4. Filippakopoulos, P.; Picaud, S.; Mangos, M.; Keates, T.; Lambert, J. P.; Barsyte-Lovejoy, D.; Felletar, I.; Volkmer, R.; Muller, S.; Pawson, T.; Gingras, A. C.; Arrowsmith, C. H.; Knapp, S. Histone recognition and large-scale structural analysis of the human bromodomain family. *Cell* **2012**, *149*, 214–231.
5. Filippakopoulos, P.; Knapp, S. Targeting bromodomains: epigenetic readers of lysine acetylation. *Nat. Rev. Drug. Discov.* **2014**, *13*, 337–356.
6. Berkovits, B. D.; Wolgemuth, D. J. The role of the double bromodomain-containing BET genes during mammalian spermatogenesis. *Curr. Top. Dev. Biol.* **2013**, *102*, 293–326.
7. Matzuk, M. M.; McKeown, M. R.; Filippakopoulos, P.; Li, Q.; Ma, L.; Agno, J. E.; Lemieux, M. E.; Picaud, S.; Yu, R. N.; Qi, J.; Knapp, S.; Bradner, J. E. Small-molecule inhibition of BRDT for male contraception. *Cell* **2012**, *150*, 673–684.

8. Jones, M. H.; Numata, M.; Shimane, M. Identification and characterization of BRDT: A testis-specific gene related to the bromodomain genes RING3 and *Drosophila* fsh. *Genomics* **1997**, *45*, 529–534.
9. Dawson, M. A.; Prinjha, R. K.; Dittmann, A.; Giotopoulos, G.; Bantscheff, M.; Chan, W. I.; Robson, S. C.; Chung, C. W.; Hopf, C.; Savitski, M. M.; Huthmacher, C.; Gudgin, E.; Lugo, D.; Beinke, S.; Chapman, T. D.; Roberts, E. J.; Soden, P. E.; Auger, K. R.; Mirguet, O.; Doehner, K.; Delwel, R.; Burnett, A. K.; Jeffrey, P.; Drewes, G.; Lee, K.; Huntly, B. J.; Kouzarides, T. Inhibition of BET recruitment to chromatin as an effective treatment for MLL-fusion leukaemia. *Nature* **2011**, *478*, 529–533.
10. Yang, Z.; Yik, J. H.; Chen, R.; He, N.; Jang, M. K.; Ozato, K.; Zhou, Q. Recruitment of P-TEFb for stimulation of transcriptional elongation by the bromodomain protein Brd4. *Mol. Cell* **2005**, *19*, 535–545.
11. Bisgrove, D. A.; Mahmoudi, T.; Henklein, P.; Verdin, E. Conserved P-TEFb-interacting domain of BRD4 inhibits HIV transcription. *Proc. Natl. Acad. Sci. USA* **2007**, *104*, 13690–13695.
12. Rahl, P. B.; Lin, C. Y.; Seila, A. C.; Flynn, R. A.; McCuine, S.; Burge, C. B.; Sharp, P. A.; Young, R. A. c-Myc regulates transcriptional pause release. *Cell* **2010**, *141*, 432–445.
13. Delmore, J. E.; Issa, G. C.; Lemieux, M. E.; Rahl, P. B.; Shi, J.; Jacobs, H. M.; Kastitis, E.; Gilpatrick, T.; Paranal, R. M.; Qi, J.; Chesi, M.; Schinzel, A. C.; McKeown, M. R.; Heffernan, T. P.; Vakoc, C. R.; Bergsagel, P. L.; Ghobrial, I. M.; Richardson, P. G.; Young, R. A.; Hahn, W. C.; Anderson, K. C.; Kung, A. L.; Bradner, J. E.; Mitsiades, C. S. BET bromodomain inhibition as a therapeutic strategy to target c-Myc. *Cell* **2011**, *146*, 904–917.

14. Loven, J.; Hoke, H. A.; Lin, C. Y.; Lau, A.; Orlando, D. A.; Vakoc, C. R.; Bradner, J. E.; Lee, T. I.; Young, R. A. Selective inhibition of tumor oncogenes by disruption of super-enhancers. *Cell* **2013**, *153*, 320–334.
15. French, C. A.; Ramirez, C. L.; Kolmakova, J.; Hickman, T. T.; Cameron, M. J.; Thyne, M. E.; Kutok, J. L.; Toretsky, J. A.; Tadavarthy, A. K.; Kees, U. R.; Fletcher, J. A.; Aster, J. C. BRD-NUT oncoproteins: a family of closely related nuclear proteins that block epithelial differentiation and maintain the growth of carcinoma cells. *Oncogene* **2008**, *27*, 2237–2242.
16. Filippakopoulos, P.; Qi, J.; Picaud, S.; Shen, Y.; Smith, W. B.; Fedorov, O.; Morse, E. M.; Keates, T.; Hickman, T. T.; Felletar, I.; Philpott, M.; Munro, S.; McKeown, M. R.; Wang, Y.; Christie, A. L.; West, N.; Cameron, M. J.; Schwartz, B.; Heightman, T. D.; La Thangue, N.; French, C. A.; Wiest, O.; Kung, A. L.; Knapp, S.; Bradner, J. E. Selective inhibition of BET bromodomains. *Nature* **2010**, *468*, 1067–1073.
17. Chaidos, A.; Caputo, V.; Gouvedenou, K.; Liu, B.; Marigo, I.; Chaudhry, M. S.; Rotolo, A.; Tough, D. F.; Smithers, N. N.; Bassil, A. K.; Chapman, T. D.; Harker, N. R.; Barbash, O.; Tummino, P.; Al-Mahdi, N.; Haynes, A. C.; Cutler, L.; Le, B.; Rahemtulla, A.; Roberts, I.; Kleijnen, M.; Witherington, J. J.; Parr, N. J.; Prinjha, R. K.; Karadimitris, A. Potent antimyeloma activity of the novel bromodomain inhibitors I-BET151 and I-BET762. *Blood* **2014**, *123*, 697–705.
18. Zuber, J.; Shi, J.; Wang, E.; Rappaport, A. R.; Herrmann, H.; Sison, E. A.; Magoon, D.; Qi, J.; Blatt, K.; Wunderlich, M.; Taylor, M. J.; Johns, C.; Chicas, A.; Mulloy, J. C.; Kogan, S. C.; Brown, P.; Valent, P.; Bradner, J. E.; Lowe, S. W.; Vakoc, C. R. RNAi screen identifies Brd4 as a therapeutic target in acute myeloid leukaemia. *Nature* **2011**, *478*, 524–528.

19. Cheng, Z.; Gong, Y.; Ma, Y.; Lu, K.; Lu, X.; Pierce, L. A.; Thompson, R. C.; Muller, S.; Knapp, S.; Wang, J. Inhibition of BET bromodomain targets genetically diverse glioblastoma. *Clin. Cancer Res.* **2013**, *19*, 1748–1759.
20. da Motta, L. L.; Ledaki, I.; Purshouse, K.; Haider, S.; De Bastiani, M. A.; Baban, D.; Morotti, M.; Steers, G.; Wigfield, S.; Bridges, E.; Li, J. L.; Knapp, S.; Ebner, D.; Klamt, F.; Harris, A. L.; McIntyre, A. The BET inhibitor JQ1 selectively impairs tumour response to hypoxia and downregulates CA9 and angiogenesis in triple negative breast cancer. *Oncogene* **2017**, *36*, 122–132.
21. Liu, Z.; Wang, P.; Chen, H.; Wold, E. A.; Tian, B.; Brasier, A. R.; Zhou, J. Drug discovery targeting bromodomain-containing protein 4. *J. Med. Chem.* **2017**, *60*, 4533–4558.
22. Tough, D. F.; Tak, P. P.; Tarakhovsky, A.; Prinjha, R. K. Epigenetic drug discovery: breaking through the immune barrier. *Nat. Rev. Drug. Discov.* **2016**, *15*, 835–853.
23. Tough, D. F.; Prinjha, R. K. Immune disease-associated variants in gene enhancers point to BET epigenetic mechanisms for therapeutic intervention. *Epigenomics* **2017**, *9*, 573–584.
24. Mele, D. A.; Salmeron, A.; Ghosh, S.; Huang, H. R.; Bryant, B. M.; Lora, J. M. BET bromodomain inhibition suppresses TH17-mediated pathology. *J. Exp. Med.* **2013**, *210*, 2181–2190.
25. Bandukwala, H. S.; Gagnon, J.; Togher, S.; Greenbaum, J. A.; Lamperti, E. D.; Parr, N. J.; Molesworth, A. M.; Smithers, N.; Lee, K.; Witherington, J.; Tough, D. F.; Prinjha, R. K.; Peters, B.; Rao, A. Selective inhibition of CD4⁺ T-cell cytokine production and autoimmunity by BET protein and c-Myc inhibitors. *Proc. Natl. Acad. Sci. USA* **2012**, *109*, 14532–14537.

26. Chan, C. H.; Fang, C.; Qiao, Y.; Yamilina, A.; Prinjha, R. K.; Ivashkiv, L. B. BET bromodomain inhibition suppresses transcriptional responses to cytokine-Jak-STAT signaling in a gene-specific manner in human monocytes. *Eur. J. Immunol.* **2015**, *45*, 287–297.
27. Schilderink, R.; Bell, M.; Reginato, E.; Patten, C.; Rioja, I.; Hilbers, F. W.; Kabala, P. A.; Reedquist, K. A.; Tough, D. F.; Tak, P. P.; Prinjha, R. K.; de Jonge, W. J. BET bromodomain inhibition reduces maturation and enhances tolerogenic properties of human and mouse dendritic cells. *Mol. Immunol.* **2016**, *79*, 66–76.
28. Belkina, A. C.; Nikolajczyk, B. S.; Denis, G. V. BET protein function is required for inflammation: Brd2 genetic disruption and BET inhibitor JQ1 impair mouse macrophage inflammatory responses. *J. Immunol.* **2013**, *190*, 3670–3678.
29. Klein, K.; Kabala, P. A.; Grabiec, A. M.; Gay, R. E.; Kolling, C.; Lin, L. L.; Gay, S.; Tak, P. P.; Prinjha, R. K.; Ospelt, C.; Reedquist, K. A. The bromodomain protein inhibitor I-BET151 suppresses expression of inflammatory genes and matrix degrading enzymes in rheumatoid arthritis synovial fibroblasts. *Ann. Rheum. Dis.* **2016**, *75*, 422–429.
30. Nicodeme, E.; Jeffrey, K. L.; Schaefer, U.; Beinke, S.; Dewell, S.; Chung, C. W.; Chandwani, R.; Marazzi, I.; Wilson, P.; Coste, H.; White, J.; Kirilovsky, J.; Rice, C. M.; Lora, J. M.; Prinjha, R. K.; Lee, K.; Tarakhovsky, A. Suppression of inflammation by a synthetic histone mimic. *Nature* **2010**, *468*, 1119–1123.
31. Meng, S.; Zhang, L.; Tang, Y.; Tu, Q.; Zheng, L.; Yu, L.; Murray, D.; Cheng, J.; Kim, S. H.; Zhou, X.; Chen, J. BET Inhibitor JQ1 blocks inflammation and bone destruction. *J. Dent. Res.* **2014**, *93*, 657–662.
32. Nadeem, A.; Al-Harbi, N. O.; Al-Harbi, M. M.; El-Sherbeeney, A. M.; Ahmad, S. F.; Siddiqui, N.; Ansari, M. A.; Zoheir, K. M.; Attia, S. M.; Al-Hosaini, K. A.; Al-Sharary, S. D. Imiquimod-induced psoriasis-like skin inflammation is suppressed by BET bromodomain

- inhibitor in mice through RORC/IL-17A pathway modulation. *Pharmacol. Res.* **2015**, *99*, 248–257.
33. Zhang, Q. G.; Qian, J.; Zhu, Y. C. Targeting bromodomain-containing protein 4 (BRD4) benefits rheumatoid arthritis. *Immunol. Lett.* **2015**, *166*, 103–108.
34. Park-Min, K. H.; Lim, E.; Lee, M. J.; Park, S. H.; Giannopoulou, E.; Yamilina, A.; van der Meulen, M.; Zhao, B.; Smithers, N.; Witherington, J.; Lee, K.; Tak, P. P.; Prinjha, R. K.; Ivashkiv, L. B. Inhibition of osteoclastogenesis and inflammatory bone resorption by targeting BET proteins and epigenetic regulation. *Nat. Commun.* **2014**, *5*, 5418.
35. Banerjee, C.; Archin, N.; Michaels, D.; Belkina, A. C.; Denis, G. V.; Bradner, J.; Sebastiani, P.; Margolis, D. M.; Montano, M. BET bromodomain inhibition as a novel strategy for reactivation of HIV-1. *J. Leukoc. Biol.* **2012**, *92*, 1147–1154.
36. Boehm, D.; Calvanese, V.; Dar, R. D.; Xing, S.; Schroeder, S.; Martins, L.; Aull, K.; Li, P. C.; Planelles, V.; Bradner, J. E.; Zhou, M. M.; Siliciano, R. F.; Weinberger, L.; Verdin, E.; Ott, M. BET bromodomain-targeting compounds reactivate HIV from latency via a Tat-independent mechanism. *Cell Cycle* **2013**, *12*, 452–462.
37. Li, Z.; Guo, J.; Wu, Y.; Zhou, Q. The BET bromodomain inhibitor JQ1 activates HIV latency through antagonizing Brd4 inhibition of Tat-transactivation. *Nucleic Acids Res.* **2013**, *41*, 277–287.
38. Picaud, S.; Wells, C.; Felletar, I.; Brotherton, D.; Martin, S.; Savitsky, P.; Diez-Dacal, B.; Philpott, M.; Bountra, C.; Lingard, H.; Fedorov, O.; Muller, S.; Brennan, P. E.; Knapp, S.; Filippakopoulos, P. RVX-208, an inhibitor of BET transcriptional regulators with selectivity for the second bromodomain. *Proc. Natl. Acad. Sci. USA* **2013**, *110*, 19754–19759.
39. McNeill, E. RVX-208, a stimulator of apolipoprotein AI gene expression for the treatment of cardiovascular diseases. *Curr. Opin. Investig. Drugs* **2010**, *11*, 357–364.

40. Sanchez, R.; Meslamani, J.; Zhou, M. M. The bromodomain: from epigenome reader to druggable target. *Biochim. Biophys. Acta.* **2014**, *1839*, 676–685.
41. Brand, M.; Measures, A. R.; Wilson, B. G.; Cortopassi, W. A.; Alexander, R.; Hoss, M.; Hewings, D. S.; Rooney, T. P.; Paton, R. S.; Conway, S. J. Small molecule inhibitors of bromodomain-acetyl-lysine interactions. *ACS Chem. Biol.* **2015**, *10*, 22–39.
42. Tough, D. F.; Lewis, H. D.; Rioja, I.; Lindon, M. J.; Prinjha, R. K. Epigenetic pathway targets for the treatment of disease: accelerating progress in the development of pharmacological tools: IUPHAR Review 11. *Br. J. Pharmacol.* **2014**, *171*, 4981–5010.
43. Zhao, Y.; Yang, C.-Y.; Wang, S. The Making of I-BET762, a BET bromodomain inhibitor now in clinical development. *J. Med. Chem.* **2013**, *56*, 7498–7500.
44. Mirguet, O.; Gosmini, R.; Toum, J.; Clement, C. A.; Barnathan, M.; Brusq, J. M.; Mordaunt, J. E.; Grimes, R. M.; Crowe, M.; Pineau, O.; Ajakane, M.; Daugan, A.; Jeffrey, P.; Cutler, L.; Haynes, A. C.; Smithers, N. N.; Chung, C. W.; Bamborough, P.; Uings, I. J.; Lewis, A.; Witherington, J.; Parr, N.; Prinjha, R. K.; Nicodeme, E. Discovery of epigenetic regulator I-BET762: lead optimization to afford a clinical candidate inhibitor of the BET bromodomains. *J. Med. Chem.* **2013**, *56*, 7501–7515.
45. Gosmini, R.; Nguyen, V. L.; Toum, J.; Simon, C.; Brusq, J. M.; Krysa, G.; Mirguet, O.; Riou-Eymard, A. M.; Boursier, E. V.; Trottet, L.; Bamborough, P.; Clark, H.; Chung, C. W.; Cutler, L.; Demont, E. H.; Kaur, R.; Lewis, A. J.; Schilling, M. B.; Soden, P. E.; Taylor, S.; Walker, A. L.; Walker, M. D.; Prinjha, R. K.; Nicodeme, E. The discovery of I-BET726 (GSK1324726A), a potent tetrahydroquinoline ApoA1 up-regulator and selective BET bromodomain inhibitor. *J. Med. Chem.* **2014**, *57*, 8111–8131.
46. Zhang, G.; Plotnikov, A. N.; Rusinova, E.; Shen, T.; Morohashi, K.; Joshua, J.; Zeng, L.; Mujtaba, S.; Ohlmeyer, M.; Zhou, M. M. Structure-guided design of potent diazobenzene inhibitors for the BET bromodomains. *J. Med. Chem.* **2013**, *56*, 9251–9264.

47. Chung, C. W.; Coste, H.; White, J. H.; Mirguet, O.; Wilde, J.; Gosmini, R. L.; Delves, C.; Magny, S. M.; Woodward, R.; Hughes, S. A.; Boursier, E. V.; Flynn, H.; Bouillot, A. M.; Bamborough, P.; Brusq, J. M.; Gellibert, F. J.; Jones, E. J.; Riou, A. M.; Homes, P.; Martin, S. L.; Uings, I. J.; Toum, J.; Clement, C. A.; Boullay, A. B.; Grimley, R. L.; Blandel, F. M.; Prinjha, R. K.; Lee, K.; Kirilovsky, J.; Nicodeme, E. Discovery and characterization of small molecule inhibitors of the BET family bromodomains. *J. Med. Chem.* **2011**, *54*, 3827–3838.
48. Gacias, M.; Gerona-Navarro, G.; Plotnikov, A. N.; Zhang, G.; Zeng, L.; Kaur, J.; Moy, G.; Rusinova, E.; Rodriguez, Y.; Matikainen, B.; Vincek, A.; Joshua, J.; Casaccia, P.; Zhou, M. M. Selective chemical modulation of gene transcription favors oligodendrocyte lineage progression. *Chem. Biol.* **2014**, *21*, 841–854.
49. Hugle, M.; Lucas, X.; Weitzel, G.; Ostrovskiy, D.; Breit, B.; Gerhardt, S.; Einsle, O.; Gunther, S.; Wohlwend, D. 4-Acyl pyrrole derivatives yield novel vectors for designing inhibitors of the acetyl-lysine recognition site of BRD4(1). *J. Med. Chem.* **2016**, *59*, 1518–1530.
50. McLure, K. G.; Gesner, E. M.; Tsujikawa, L.; Kharenko, O. A.; Attwell, S.; Campeau, E.; Wasiak, S.; Stein, A.; White, A.; Fontano, E.; Suto, R. K.; Wong, N. C.; Wagner, G. S.; Hansen, H. C.; Young, P. R. RVX-208, an inducer of ApoA-I in humans, is a BET bromodomain antagonist. *PLoS One* **2013**, *8*, e83190.
51. Kharenko, O. A.; Gesner, E. M.; Patel, R. G.; Norek, K.; White, A.; Fontano, E.; Suto, R. K.; Young, P. R.; McLure, K. G.; Hansen, H. C. RVX-297- a novel BD2 selective inhibitor of BET bromodomains. *Biochem. Biophys. Res. Commun.* **2016**, *477*, 62–67.
52. Jahagirdar, R.; Attwell, S.; Marusic, S.; Bendele, A.; Shenoy, N.; McLure, K. G.; Gilham, D.; Norek, K.; Hansen, H. C.; Yu, R.; Tobin, J.; Wagner, G. S.; Young, P. R.; Wong, N. C.; Kulikowski, E. RVX-297, a BET bromodomain inhibitor, has therapeutic effects in

preclinical models of acute inflammation and autoimmune disease. *Mol. Pharmacol.* **2017**, 92, 694–706.

53. Wang, Q.; Li, Y.; Xu, J.; Wang, Y.; Leung, E. L.; Liu, L.; Yao, X. Selective inhibition mechanism of RVX-208 to the second bromodomain of bromo and extraterminal proteins: insight from microsecond molecular dynamics simulations. *Sci. Rep.* **2017**, 7, 8857.

54. Cheng, C.; Diao, H.; Zhang, F.; Wang, Y.; Wang, K.; Wu, R. Deciphering the mechanisms of selective inhibition for the tandem BD1/BD2 in the BET-bromodomain family. *Phys. Chem. Chem. Phys.* **2017**, 19, 23934–23941.

55. Baud, M. G.; Lin-Shiao, E.; Cardote, T.; Tallant, C.; Pschibul, A.; Chan, K. H.; Zengerle, M.; Garcia, J. R.; Kwan, T. T.; Ferguson, F. M.; Ciulli, A. Chemical biology. A bump-and-hole approach to engineer controlled selectivity of BET bromodomain chemical probes. *Science* **2014**, 346, 638–641.

56. Baud, M. G.; Lin-Shiao, E.; Zengerle, M.; Tallant, C.; Ciulli, A. New synthetic routes to triazolo-benzodiazepine analogues: expanding the scope of the bump-and-hole approach for selective bromo and extra-terminal (BET) bromodomain inhibition. *J. Med. Chem.* **2016**, 59, 1492–1500.

57. Albrecht, B. K.; Gehling, V. S.; Hewitt, M. C.; Vaswani, R. G.; Cote, A.; Leblanc, Y.; Nasveschuk, C. G.; Bellon, S.; Bergeron, L.; Campbell, R.; Cantone, N.; Cooper, M. R.; Cummings, R. T.; Jayaram, H.; Joshi, S.; Mertz, J. A.; Neiss, A.; Normant, E.; O'Meara, M.; Pardo, E.; Poy, F.; Sandy, P.; Supko, J.; Sims, R. J., 3rd; Harmange, J. C.; Taylor, A. M. Audia, J. E. Identification of a benzoisoxazoloazepine inhibitor (CPI-0610) of the bromodomain and extra-terminal (BET) family as a candidate for human clinical trials. *J. Med. Chem.* **2016**, 59, 1330–1339.

58. Wang, L.; Dai, Y.; Holms, J.; Liu, D.; McClellan, W.; McDaniel, K.; Hasvold, L.; Fidanze, S. D.; Sheppard, G.; Marjanovic, J. Bromodomain inhibitors. WO2014206345A1, 2014.
59. McDaniel, K. F.; Wang, L.; Soltwedel, T.; Fidanze, S. D.; Hasvold, L. A.; Liu, D.; Mantei, R. A.; Pratt, J. K.; Sheppard, G. S.; Bui, M. H.; Faivre, E. J.; Huang, X.; Li, L.; Lin, X.; Wang, R.; Warder, S. E.; Wilcox, D.; Albert, D. H.; Magoc, T. J.; Rajaraman, G.; Park, C. H.; Hutchins, C. W.; Shen, J. J.; Edalji, R. P.; Sun, C. C.; Martin, R.; Gao, W.; Wong, S.; Fang, G.; Elmore, S. W.; Shen, Y.; Kati, W. M. Discovery of *N*-(4-(2,4-difluorophenoxy)-3-(6-methyl-7-oxo-6,7-dihydro-1*H*-pyrrolo[2,3-*c*]pyridin-4-yl)phenyl)ethanesulfonamide (ABBV-075/Mivebresib), a potent and orally available bromodomain and extraterminal domain (BET) family bromodomain inhibitor. *J. Med. Chem.* **2017**, *60*, 8369-8384.
60. Raux, B.; Voitovich, Y.; Derviaux, C.; Lugari, A.; Rebuffet, E.; Milhas, S.; Priet, S.; Roux, T.; Trinquet, E.; Guillemot, J. C.; Knapp, S.; Brunel, J. M.; Fedorov, A. Y.; Collette, Y.; Roche, P.; Betzi, S.; Combes, S.; Morelli, X. Exploring selective inhibition of the first bromodomain of the human bromodomain and extra-terminal domain (BET) proteins. *J. Med. Chem.* **2016**, *59*, 1634–1641.
61. Sweis, R. F. Target (in)validation: a critical, sometimes unheralded, role of modern medicinal chemistry. *ACS Med. Chem. Lett.* **2015**, *6*, 618–621.
62. Chung, C. W.; Dean, A. W.; Woolven, J. M.; Bamborough, P. Fragment-based discovery of bromodomain inhibitors part 1: inhibitor binding modes and implications for lead discovery. *J. Med. Chem.* **2012**, *55*, 576–586.
63. Bair, K. W.; Herbertz, T.; Kauffman, G. S.; Kayser-Bricker, K. J.; Luke, G. P.; Martin, M. W.; Millan, D. S.; Schiller, S. E. R.; Talbot, A. C.; Tebbe, M. J. Benzopiperazine compositions as BET bromodomain inhibitors. WO2015074081A1, 2015.

64. Millan, D. S.; Kayser-Bricker, K. J.; Martin, M. W.; Talbot, A. C.; Schiller, S. E. R.; Herbertz, T.; Williams, G. L.; Luke, G. P.; Hubbs, S.; Alvarez Morales, M. A.; Cardillo, D.; Troccolo, P.; Mendes, R. L.; McKinnon, C. Design and optimization of benzopiperazines as potent inhibitors of BET bromodomains. *ACS Med. Chem. Lett.* **2017**, *8*, 847–852.
65. Amans, D.; Atkinson, S. J.; Harrison, L. A.; Hirst, D. J.; Law, R. P.; Lindon, M.; Preston, A.; Seal, J. T.; Wellaway, C. R. 2,3-disubstituted 1-acyl-4-amino-1,2,3,4-tetrahydroquinoline derivatives and their use as bromodomain inhibitors. WO2014140076A1, 2014.
66. Shadrick, W. R.; Slavish, P. J.; Chai, S. C.; Waddell, B.; Connelly, M.; Low, J. A.; Tallant, C.; Young, B. M.; Bharatham, N.; Knapp, S.; Boyd, V. A.; Morfouace, M.; Roussel, M. F.; Chen, T.; Lee, R. E.; Kiplin Guy, R.; Shelat, A. A.; Potter, P. M. Exploiting a water network to achieve enthalpy-driven, bromodomain-selective BET inhibitors. *Bioorg. Med. Chem.* **2018**, *26*, 25-36.
67. Parker, W. L.; Hanson, R. L.; Goldberg, S. L.; Tully, T. P.; Goswami, A. Preparation of (S)-1-cyclopropyl-2-methoxyethanamine by a chemoenzymatic route using leucine dehydrogenase. *Org. Process Res. Dev.* **2012**, *16*, 464–469.
68. Tanimori, S.; Kashiwagi, H.; Nishimura, T.; Kiriata, M. A general and practical access to chiral quinoxalinones with low copper-catalyst loading. *Advanced Synthesis & Catalysis* **2010**, *352*, 2531–2537.
69. Young, R. J.; Green, D. V.; Luscombe, C. N.; Hill, A. P. Getting physical in drug discovery II: the impact of chromatographic hydrophobicity measurements and aromaticity. *Drug Discovery Today* **2011**, *16*, 822–830.
70. Leeson, P. D.; Springthorpe, B. The influence of drug-like concepts on decision-making in medicinal chemistry. *Nat. Rev. Drug. Discov.* **2007**, *6*, 881–890.

71. Ritchie, T. J.; Macdonald, S. J. The impact of aromatic ring count on compound developability--are too many aromatic rings a liability in drug design? *Drug Discovery Today* **2009**, *14*, 1011–1020.
72. Ritchie, T. J.; Macdonald, S. J.; Young, R. J.; Pickett, S. D. The impact of aromatic ring count on compound developability: further insights by examining carbo- and hetero-aromatic and -aliphatic ring types. *Drug Discovery Today* **2011**, *16*, 164–171.
73. Fabian, M. A.; Biggs, W. H., 3rd; Treiber, D. K.; Atteridge, C. E.; Azimioara, M. D.; Benedetti, M. G.; Carter, T. A.; Ciceri, P.; Edeen, P. T.; Floyd, M.; Ford, J. M.; Galvin, M.; Gerlach, J. L.; Grotzfeld, R. M.; Herrgard, S.; Insko, D. E.; Insko, M. A.; Lai, A. G.; Lelias, J. M.; Mehta, S. A.; Milanov, Z. V.; Velasco, A. M.; Wodicka, L. M.; Patel, H. K.; Zarrinkar, P. P.; Lockhart, D. J. A small molecule-kinase interaction map for clinical kinase inhibitors. *Nat Biotechnol* **2005**, *23*, 329–336.
74. Blaszykowski, C.; Aktoudianakis, E.; Alberico, D.; Bressy, C.; Hulcoop, D. G.; Jafarpour, F.; Joushaghani, A.; Laleu, B.; Lautens, M. A palladium-catalyzed alkylation/direct arylation synthesis of nitrogen-containing heterocycles. *J. Org. Chem.* **2008**, *73*, 1888–1897.
75. Valko, K.; Nunhuck, S.; Bevan, C.; Abraham, M. H.; Reynolds, D. P. Fast gradient HPLC method to determine compounds binding to human serum albumin. Relationships with octanol/water and immobilized artificial membrane lipophilicity. *J. Pharm. Sci.* **2003**, *92*, 2236–2248.
76. Camurri, G.; Zaramella, A. High-throughput liquid chromatography/mass spectrometry method for the determination of the chromatographic hydrophobicity index. *Anal. Chem.* **2001**, *73*, 3716–3722.
77. Ballell, L.; Bates, R. H.; Young, R. J.; Alvarez-Gomez, D.; Alvarez-Ruiz, E.; Barroso, V.; Blanco, D.; Crespo, B.; Escribano, J.; Gonzalez, R.; Lozano, S.; Huss, S.; Santos-

- Villarejo, A.; Martin-Plaza, J. J.; Mendoza, A.; Rebollo-Lopez, M. J.; Remuinan-Blanco, M.; Lavandera, J. L.; Perez-Herran, E.; Gamo-Benito, F. J.; Garcia-Bustos, J. F.; Barros, D.; Castro, J. P.; Cammack, N. Fueling open-source drug discovery: 177 small-molecule leads against tuberculosis. *ChemMedChem* **2013**, *8*, 313–321.
78. Demont, E. H.; Bamborough, P.; Chung, C. W.; Craggs, P. D.; Fallon, D.; Gordon, L. J.; Grandi, P.; Hobbs, C. I.; Hussain, J.; Jones, E. J.; Le Gall, A.; Michon, A. M.; Mitchell, D. J.; Prinjha, R. K.; Roberts, A. D.; Sheppard, R. J.; Watson, R. J. 1,3-Dimethyl benzimidazolones are potent, selective inhibitors of the BRPF1 bromodomain. *ACS Med. Chem. Lett.* **2014**, *5*, 1190–1195.
79. Battye, T. G.; Kontogiannis, L.; Johnson, O.; Powell, H. R.; Leslie, A. G. iMOSFLM: a new graphical interface for diffraction-image processing with MOSFLM. *Acta. Crystallogr. D. Biol. Crystallogr.* **2011**, *67*, 271–281.
80. Collaborative Computational Project, N. The CCP4 suite: programs for protein crystallography. *Acta. Crystallogr. D. Biol. Crystallogr.* **1994**, *50*, 760–763.
81. Winn, M. D.; Ballard, C. C.; Cowtan, K. D.; Dodson, E. J.; Emsley, P.; Evans, P. R.; Keegan, R. M.; Krissinel, E. B.; Leslie, A. G.; McCoy, A.; McNicholas, S. J.; Murshudov, G. N.; Pannu, N. S.; Potterton, E. A.; Powell, H. R.; Read, R. J.; Vagin, A.; Wilson, K. S. Overview of the CCP4 suite and current developments. *Acta. Crystallogr. D. Biol. Crystallogr.* **2011**, *67*, 235–242.
82. Murshudov, G. N.; Vagin, A. A.; Lebedev, A.; Wilson, K. S.; Dodson, E. J. Efficient anisotropic refinement of macromolecular structures using FFT. *Acta. Crystallogr. D. Biol. Crystallogr.* **1999**, *55*, 247–255.
83. Murshudov, G. N.; Skubak, P.; Lebedev, A. A.; Pannu, N. S.; Steiner, R. A.; Nicholls, R. A.; Winn, M. D.; Long, F.; Vagin, A. A. REFMAC5 for the refinement of macromolecular crystal structures. *Acta. Crystallogr. D. Biol. Crystallogr.* **2011**, *67*, 355–367.

- 1
2
3 84. Emsley, P.; Lohkamp, B.; Scott, W. G.; Cowtan, K. Features and development of
4 Coot. *Acta. Crystallogr. D. Biol. Crystallogr.* **2010**, *66*, 486–501.
5
6
7 85. Kabsch, W. Xds. *Acta. Crystallogr. D. Biol. Crystallogr.* **2010**, *66*, 125–132.
8
9 86. Kabsch, W. Integration, scaling, space-group assignment and post-refinement. *Acta.*
10 *Crystallogr. D. Biol. Crystallogr.* **2010**, *66*, 133–144.
11
12
13 87. Baell, J. B.; Holloway, G. A. New substructure filters for removal of pan assay
14 interference compounds (PAINS) from screening libraries and for their exclusion in
15
16
17
18 bioassays. *J. Med. Chem.* **2010**, *53*, 2719–2740.
19
20
21
22
23
24
25
26
27
28
29
30
31
32
33
34
35
36
37
38
39
40
41
42
43
44
45
46
47
48
49
50
51
52
53
54
55
56
57
58
59
60

Table of Contents Graphic

